Article

Cell Reports

Characterizing Speed Cells in the Rat Hippocampus

Graphical Abstract

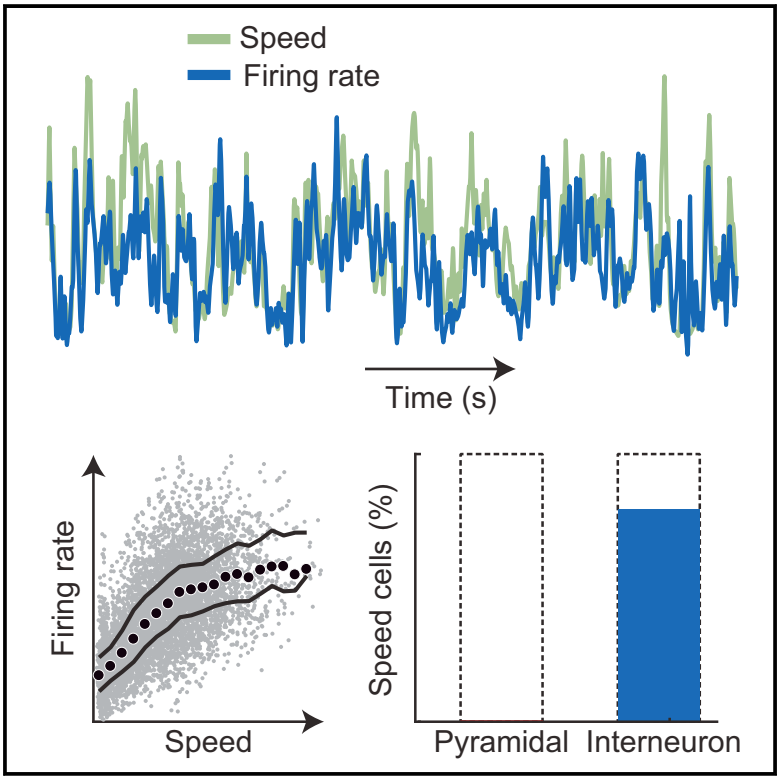

Authors

Zé Henrique T.D. Góis, Adriano B.L. Tort

Correspondence

tort@neuro.ufrn.br

In Brief

Neurons coding for locomotion speed are theoretically required to perform path integration. Góis and Tort show that in CA1, speed is encoded by inhibitory interneurons, but not pyramidal cells, shedding light on the network mechanisms of spatial navigation.

Highlights

- The firing rate of a subset of CA1 neurons highly correlates with speed
- The rate coding of CA1 speed cells is stable across space, time, and context
- CA1 speed cells are inhibitory interneurons
- Pyramidal cells are modulated by but do not encode speed on a sub-second timescale

Góis & Tort, 2018, Cell Reports *25*, 1872–1884
November 13, 2018
https://doi.org/10.1016/j.celrep.2018.10.054

CellPress

OPEN ACCESS
CellPress

Cell Reports
Article

Characterizing Speed Cells in the Rat Hippocampus

Zé Henrique T.D. Góis[1] and Adriano B.L. Tort[1,2,*]
[1]Brain Institute, Federal University of Rio Grande do Norte, Natal, RN 59056-450, Brazil
[2]Lead Contact
*Correspondence: tort@neuro.ufrn.br
https://doi.org/10.1016/j.celrep.2018.10.054

SUMMARY

Spatial navigation relies on visual landmarks as well as on self-motion information. In familiar environments, both place and grid cells maintain their firing fields in darkness, suggesting that they continuously receive information about locomotion speed required for path integration. Consistently, "speed cells" have been previously identified in the hippocampal formation and characterized in detail in the medial entorhinal cortex. Here we investigated speed-correlated firing in the hippocampus. We show that CA1 has speed cells that are stable across contexts, position in space, and time. Moreover, their speed-correlated firing occurs within theta cycles, independently of theta frequency. Interestingly, a physiological classification of cell types reveals that all CA1 speed cells are inhibitory. In fact, while speed modulates pyramidal cell activity, only the firing rate of interneurons can accurately predict locomotion speed on a sub-second timescale. These findings shed light on network models of navigation.

INTRODUCTION

The ability to navigate across space is crucial for the survival of several species. To that end, the brain must be able to construct representations of past, present, and future locations and continuously compute information about the self and the environment (Ferbinteanu and Shapiro, 2003; Dragoi and Buzsáki, 2006; Buckner, 2010; Buzsáki and Moser, 2013; Sanders et al., 2015). Current theories on spatial navigation assert that the brain uses two mechanisms for spatial coding: one conveying sensory inputs from environment landmarks (allocentric navigation) and another based on path integration or "dead reckoning" (O'Keefe, 1976; McNaughton et al., 1996; Whishaw and Brooks, 1999; Buzsáki and Moser, 2013). The latter does not depend on external stimuli but on integrating information about previous location, movement direction, and locomotion speed (egocentric navigation) (Whishaw, 1998; Buzsáki, 2005; McNaughton et al., 2006).

During the last decades, several neuronal correlates of spatial navigation have been discovered and localized to specific brain regions (Moser et al., 2008; Grieves and Jeffery, 2017). Among them, the best-known examples are the place cells in the hippocampus (O'Keefe and Dostrovsky, 1971) and the grid cells in the medial entorhinal cortex (Hafting et al., 2005). Given their periodically repeating pattern of spatial firing, grid cells have been suggested to take part in path integration (Hafting et al., 2005; Fuhs and Touretzky, 2006; McNaughton et al., 2006). Consistent with this, neurons coding for speed have been previously found in the medial entorhinal cortex (Sargolini et al., 2006; Wills et al., 2012) and recently studied in more detail (Kropff et al., 2015; Hinman et al., 2016; Ye et al., 2018). Place cells, on the other hand, would signal allocentric spatial relationships, and the primary drive for their place-selective firing would stem from sensory information such as visual landmarks (O'Keefe and Conway, 1978; O'Keefe and Speakman, 1987). Evidence for this comes from experiments showing that place fields shift coherently along with changes in the orientation of spatial cues (O'Keefe and Conway, 1978; Muller and Kubie, 1987; Sharp et al., 1990). Nevertheless, place cells also exhibit place-selective firing in darkness when animals explore familiar environments (McNaughton et al., 1989; Quirk et al., 1990), suggesting that they are also capable of keeping track of animal position using self-motion information (McNaughton et al., 1996; Knierim et al., 1998).

Adjacent structures of the hippocampal formation and the medial septum are likely to convey the hippocampus with information about head direction and locomotion speed (Taube et al., 1990; Lever et al., 2003; Hafting et al., 2005; McNaughton et al., 2006; Fuhrmann et al., 2015; Ye et al., 2018). Similar to the medial entorhinal cortex (Sargolini et al., 2006; Wills et al., 2012), hippocampal neurons have also been shown to exhibit spiking activity correlated with speed (McNaughton et al., 1983; Wiener et al., 1989; O'Keefe et al., 1998; Zhang et al., 1998; Czurkó et al., 1999, 2011; Hirase et al., 1999; Ekstrom et al., 2001; Nitz and McNaughton, 2004; Maurer et al., 2005). These previous studies, however, typically reported *average* neuronal firing rates as a function of speed and did not consider whether hippocampal neurons would code for speed on a short timescale, nor did they investigate the robustness of hippocampal speed coding across time, space, and contexts. Of note, though mostly focused on entorhinal cortex neurons, the study of Kropff et al. (2015) has also reported speed cells with similar characteristics in the hippocampus.

Given the renewed interest in speed coding in the entorhinal-hippocampal network (Kropff et al., 2015; Hinman et al., 2016; Ye et al., 2018), in the present work we sought to perform a thorough characterization of speed-correlated firing in the hippocampus. Our results confirm and expand previous reports by showing that (1) speed cells exist in the dorsal CA1, (2) speed coding by the firing rate of CA1 neurons is stable across space, elapsed time, and contexts, (3) CA1 speed coding occurs within theta cycles, and (4) CA1 speed cells exclusively comprise

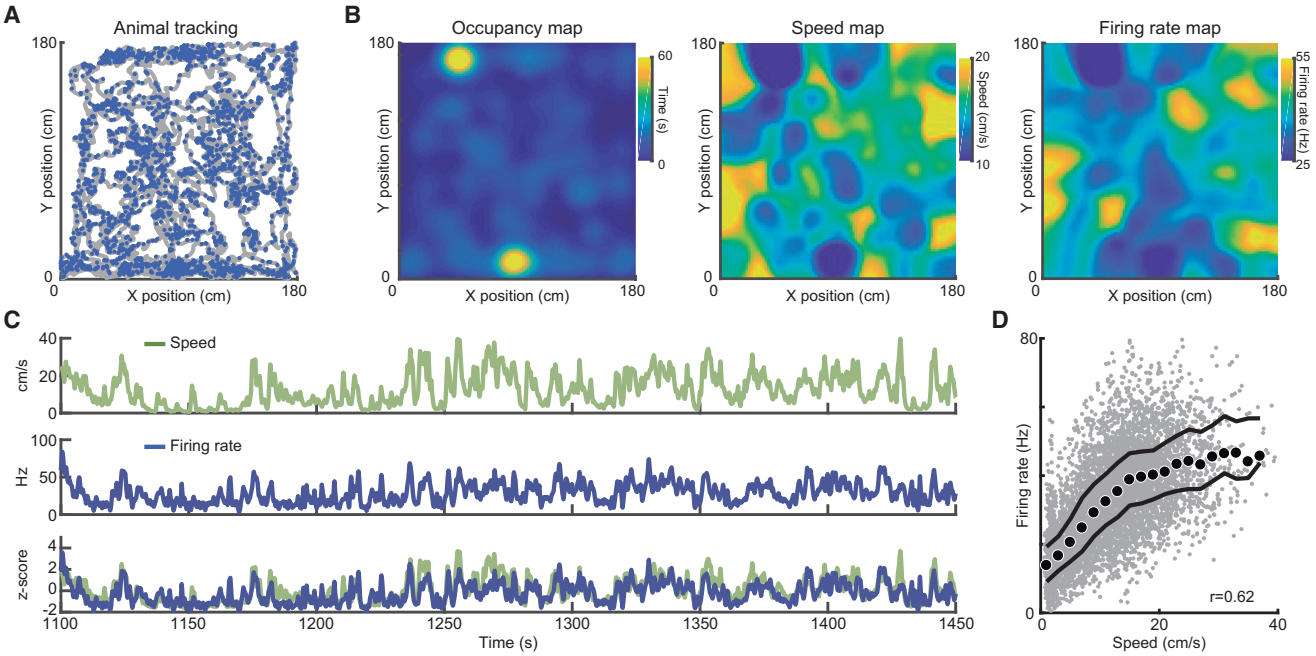

Figure 1. Speed Coding by Firing Rate in Dorsal CA1

(A) Gray line depicts animal trajectory in a square open-field arena, and blue dots show 10% of spikes selected at random from an individual CA1 neuron (session ec013.198).

(B) Spatial heatmaps of occupancy, animal speed, and firing rate for the same neuron and session.

(C) The top two panels show the time series of animal speed and neuron firing rate, respectively. The bottom panel shows the same in units of *Z* score.

(D) Scatterplot of animal speed versus neuron firing rate (gray dots; only 10% of data shown). The black circles and lines show the median and the 25%–75% quartiles for each speed bin. Inset text shows the Pearson's r ($p < 10^{-20}$), which defines the "speed score" of the cell.

interneurons. While the latter finding contrasts with previous reports showing speed-correlated firing of hippocampal pyramidal cells (e.g., McNaughton et al., 1983; Wiener et al., 1989; Czurkó et al., 1999; Hirase et al., 1999; Ekstrom et al., 2001; Maurer et al., 2005), here we demonstrate that in open fields, such correlations are only apparent when averaging firing rate values over fixed speed bins, but not on the finer timescale of animal behavior. Consistently, (5) only the firing rate of interneurons, but not of pyramidal cells, accurately predicts locomotion speed in the open field on a sub-second timescale. Moreover, we further show that (6) although pyramidal cells exhibit speed-correlated firing in a linear track task, such correlations can be explained by spatial coding along with the interdependence of space and speed due to the nature of the task (i.e., animals stereotypically run fastest in the middle of the linear track and slowest on the edges). Our findings thus show that while speed may modulate CA1 pyramidal cell activity, it is only truly encoded by the firing rate of inhibitory interneurons.

RESULTS

Speed Cells in the Dorsal CA1

To search for the neuronal correlates of locomotion speed in the dorsal hippocampus, we analyzed the activity of CA1 single units while freely moving rats (n = 3 animals) wandered in a square open-field arena (n = 62 sessions) or ran back and forth on a linear track (n = 101 sessions). Figure 1A shows a representative example of an animal trajectory in the square arena plotted along with 10% of the spikes of a CA1 neuron; note that this neuron fired all over the arena. Figure 1B depicts by means of heatmaps the time the animal spent on each position of the square arena, its average locomotion speed, and the spatial firing rate map of the neuron. In this session, the animal spent most of the time in two different locations, noticeable by either the warm colors in the spatial occupancy map, which indicate large occupancy times, or the cold colors in the spatial speed map, which indicate low speeds. Interestingly, the firing rate of the example neuron was also lowest at these same locations, suggesting that locomotion speed modulated its spiking activity. To investigate this possibility, we computed time series of locomotion speed and firing rate (see Method Details in STAR Methods). As shown in Figure 1C, visual inspection of the time series revealed remarkably similar variations in speed and firing rate. Pearson's correlation analysis confirmed a highly significant linear correlation between these variables ($r = 0.62$, $p < 10^{-20}$; Figure 1D). As in previous work (Kropff et al., 2015), we define the speed score of a neuron as the Pearson's correlation coefficient between the time series of its firing rate and locomotion speed. Therefore, in this square arena session, the example neuron had a speed score of 0.62 (Figure 1D).

Figure 2 shows a second example of a CA1 neuron driven by speed in another animal during a 90-min-long session in the square arena. Similar to the previous example, there is a clear resemblance between the spatial distribution of speed and

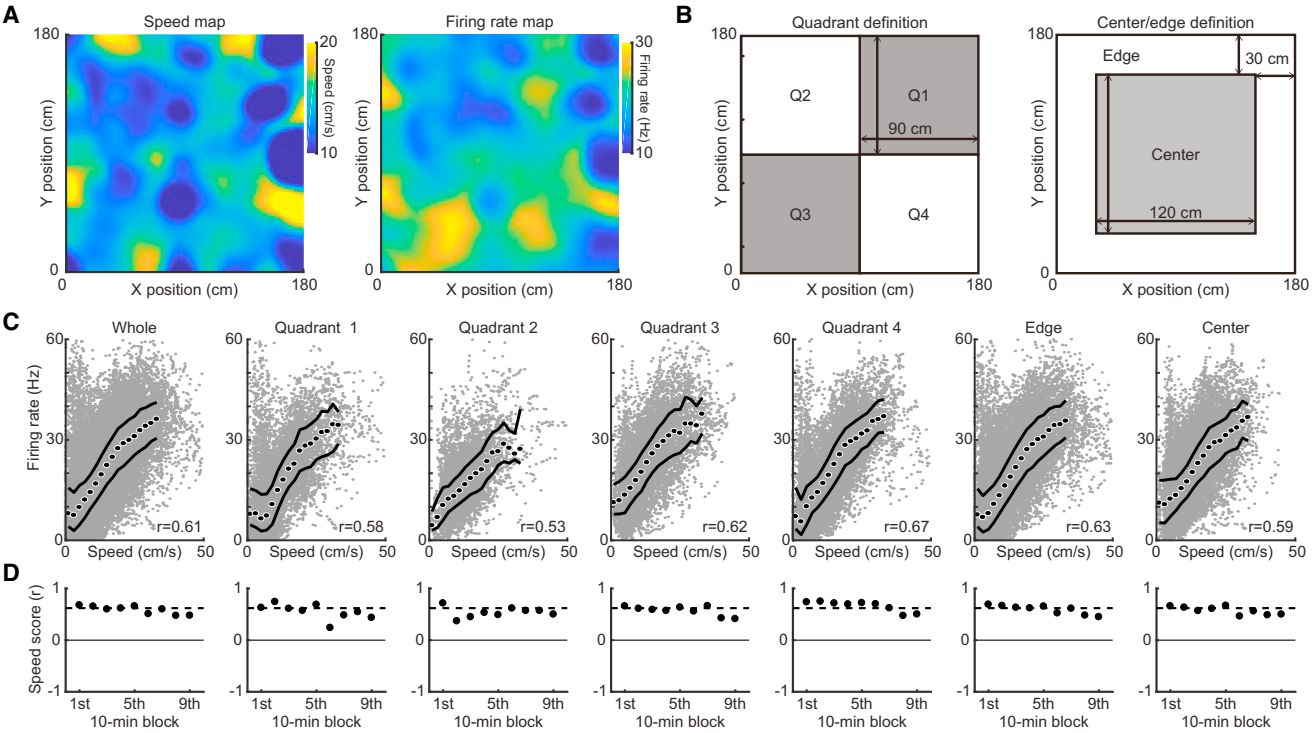

Figure 2. Speed Coding in Dorsal CA1 Is Stable across Space and Time

(A) Spatial heatmaps of animal speed and of a CA1 neuron firing rate (session ec014.277).

(B) Definition of quadrants (left) and edge and center (right) subregions of the square open-field arena.

(C) Scatterplot of animal speed versus firing rate in the arena subregions (same neuron as in A). Black circles and lines show median and 25%–75% quartiles for each speed bin. Inset texts are speed scores (all p values < 10^{-20}).

(D) Speed scores in non-overlapping 10-min blocks (all p values < 10^{-13}). Different panels show results for different arena subregions, as labeled in (C).

neuronal firing rate (Figure 2A). The correlation between firing rate and locomotion speed using data from the whole session revealed a speed score of 0.61 (Figure 2C, leftmost panel). To test if the speed coding of this neuron depended on spatial location, we divided the square arena into six subregions (Figure 2B) and computed correlation coefficients between firing rate and locomotion speed (i.e., speed scores) using only periods in which the animal was inside each subregion. As shown in Figure 2C, the firing rate of the neuron correlated with speed within all arena subregions. Moreover, speed scores were remarkably similar, ranging from 0.53 to 0.67. This result indicates that the firing rate of this CA1 neuron coded for speed alone and not for particular features of the arena. We next investigated whether speed coding would depend on the time elapsed since the beginning of the session. Correlations between speed and firing rate computed for nine non-overlapping 10-min blocks revealed stable speed scores across the session (Figure 2D, leftmost panel). Moreover, speed scores were also stable when further restricting the time block analysis to each arena subregion (Figure 2D). Therefore, the speed coding by firing rate was stable across space and time.

The example neurons in Figures 1 and 2 are representative of a subpopulation of CA1 neurons, hereafter referred to as "speed cells." Namely, the distribution of speed scores across all 644 CA1 neurons with average firing rate > 0.3 Hz in the square arena was bimodal, with a prominent peak near 0 and a smaller bump centered around 0.45 (Figure 3A). Interestingly, a small minority of cells exhibited negative speed scores. Figure 3B shows three examples of surrogate distributions of speed scores (see Method Details) along with the actual speed score for cells whose firing rate had non-significant (top), negative (middle), and positive (bottom) correlations with speed. At the group level, the observed distribution of speed scores was skewed to the right compared to the pooled distribution of surrogate speed scores (Figure 3A). In this work, we operationally defined speed cells as neurons having absolute speed score greater than 0.3. Note that this threshold is much more conservative than a definition solely based on surrogate distributions (Figures 3A and 3B). The choice of this conservative threshold was justified because (1) it separated well the large and small peaks in the actual distribution of speed scores (Figure 3A); (2) all absolute speed scores above this threshold were highly significant when compared to surrogate distributions; and (3) we wanted to avoid spurious correlations due to spatial influences such as place field traversals. (Clearly, place cells spike at higher rates when the animal runs across the place field than during immobility; in turn, this leads to weak correlations between firing rate and speed that are deemed significant by surrogate-based statistics.) Under this more stringent definition, we found that 93/644 (14%) of CA1 neurons were speed cells. As the example cell in Figure 2, the

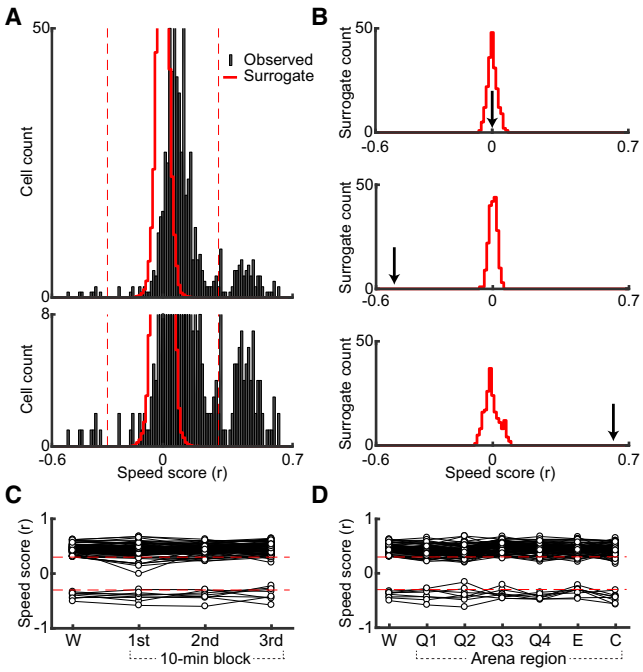

Figure 3. Operational Definition of CA1 Speed Cells

(A) Distribution of speed scores for 644 CA1 neurons with average firing rate > 0.3 Hz in the square open-field arena (black bars). Also shown is the pooled surrogate distribution of speed scores obtained from time-shifted data (continuous red line). Speed cells were defined as neurons with absolute speed score greater than 0.3 (dashed red lines). The bottom panel depicts a zoomed-in view.

(B) Surrogate distributions of speed scores of three individual neurons (red lines). The actual scores are also shown (black arrow).

(C) Speed scores for all CA1 speed cells for the whole session (W) and computed within the first, middle, and last 10-min block of exploration in the square open-field arena.

(D) Speed scores for all CA1 speed cells within subregions of the square arena (see Figure 2B). Q, quadrant; E, edge; C, center.

vast majority of defined speed cells were stable across time (Figure 3C) and space (Figure 3D).

Speed Coding within Theta Cycles

Theta oscillations (5–10 Hz) robustly appear in hippocampal local field potentials (LFPs) when rats perform voluntary movements (Buzsáki, 2005; Buzsáki and Moser, 2013). Previous studies have shown that the frequency of the LFP theta rhythm increases with locomotion speed (Sławińska and Kasicki, 1998; Hinman et al., 2011). Moreover, it has also been well documented that the spiking activity of hippocampal neurons may oscillate at theta frequency and that the LFP theta phase modulates spiking probability (Frank et al., 2001; Buzsáki, 2002; Klausberger et al., 2003). Therefore, the changes in the firing rate of CA1 speed cells may relate to the changes in theta frequency with speed, in which a higher number of theta cycles per unit of time would consequentially lead to a higher number of spikes per unit of time, an effect referred to as ''oscillatory coding'' (Hinman et al., 2016). Alternatively, the increase in firing rate with speed could also occur within theta cycles. In this scenario, CA1 speed cells would emit more spikes per theta cycle as a function of speed irrespective of theta frequency, which defines ''rate coding'' (Hinman et al., 2016). We next investigated whether rate coding would underlie the firing rate changes of CA1 speed cells.

The top panel of Figure 4A shows the standard autocorrelogram of a CA1 speed cell exhibiting theta-rhythmic firing, and the middle panel shows the speed-binned auto-correlogram, which depicts normalized spiking probabilities for different speeds (see Method Details). Notice that theta-rhythmic firing by this neuron occurred at all speeds. Moreover, as with the LFP theta rhythm (Figure 4A, bottom panel), theta-rhythmic firing increased in frequency with speed (as inferred from the shorter period between the probability peaks), suggestive of oscillatory coding (Hinman et al., 2016). Nevertheless, to test for rate coding, we next counted the number spikes emitted per theta cycle when controlling for locomotion speed. As shown in Figure 4B, the spike count per theta cycle increased with animal speed; moreover, such increase was proportional to the increase in firing rate with speed. This example neuron is representative of the population of CA1 speed cells. Namely, at the group level, we found that the slope of spike counts per theta cycle versus speed was positive and highly correlated with the slope of firing rate versus speed ($r = 0.98$, $p < 10^{-40}$) (Figure 4C). Therefore, we conclude that CA1 speed cells display a genuine rate coding of speed: their firing rate increases proportional to locomotion speed irrespective of changes in LFP theta frequency.

CA1 Speed Cells Are Interneurons

The firing rate maps of the representative CA1 speed cells in Figures 1 and 2 show that spikes occurred all over the square open-field arena. Moreover, notice in the scatterplots of Figures 1, 2, and 4 that all example CA1 speed cells displayed high firing rate. Low spatial selectively and high firing rate characterize the spiking activity of inhibitory interneurons in CA1 (Frank et al., 2001). In contrast, CA1 pyramidal cells tend to emit low-frequency spikes with higher spatial information (McNaughton et al., 1983; Frank et al., 2001). These observations strongly suggest that CA1 speed cells are interneurons. To investigate this possibility, we used an identification of pyramidal cells and interneurons based on spike cross-correlograms (CCGs) (Figure 5A; Fujisawa et al., 2008; Mizuseki et al., 2009). Figures 5B–5F show results obtained for all pyramidal neurons and interneurons recorded in the square open-field arena that could be identified under the CCG analysis. As expected, neurons physiologically identified as interneurons had a higher firing rate and narrower spike width than neurons identified as pyramidal cells (Figure 5B). Interestingly, we found that virtually all CA1 units classified as speed cells in the square arena were interneurons (Figures 5C–5F). Accordingly, from a total of 77 cells physiologically identified as CA1 interneurons, 61 (79%) were considered speed cells. In contrast, only 1 of the 279 (0.36%) physiologically identified pyramidal cells was classified as speed cell in the square arena (Figure 5F).

Cross-correlations between the time series of firing rate and locomotion speed further revealed that the firing rate changes of CA1 speed cells lagged changes in speed by 64.8 ± 22.9 ms, which was significantly different from zero ($t(61) = -2.826$, $p = 0.0064$; Figure S1). On the other hand,

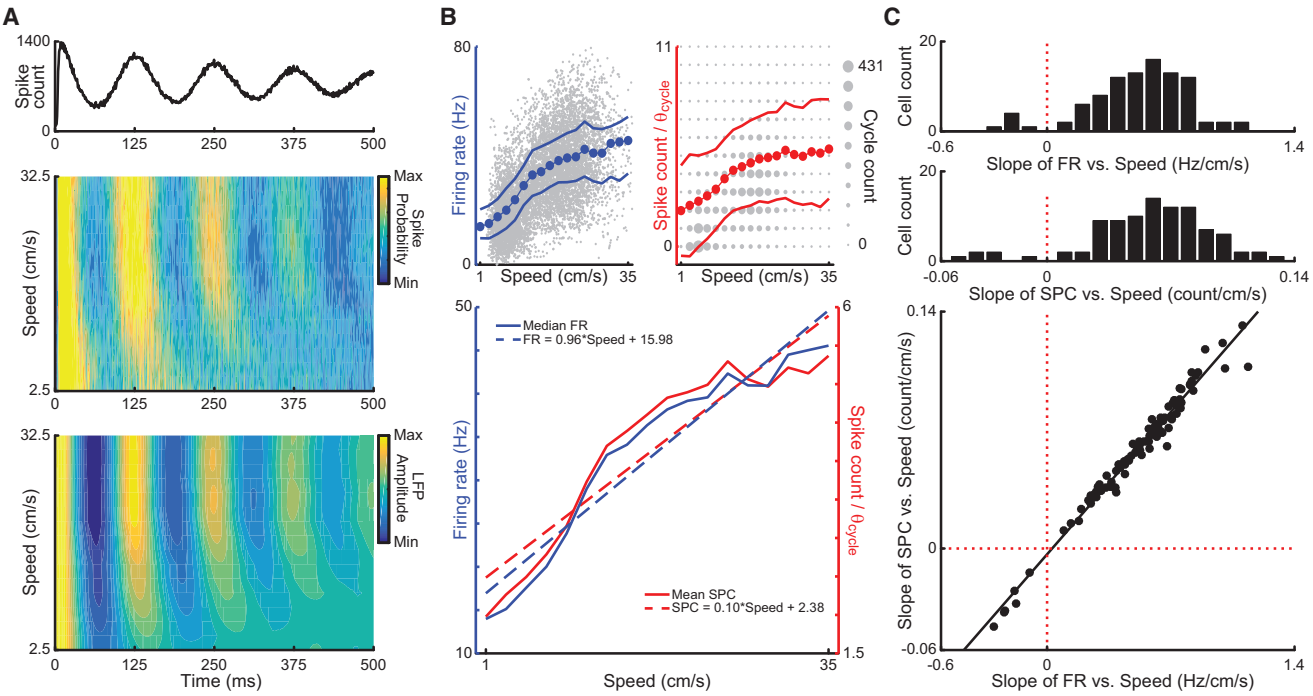

Figure 4. Speed Cells Spike More per Theta Cycle with Speed

(A) Standard (top) and speed-binned (middle) autocorrelograms of a CA1 speed cell; the speed-binned LFP autocorrelogram is also shown (bottom).

(B) The top panels show scatterplots of firing rate (FR, left) versus speed and of spikes per theta cycle (SPC, right) versus speed for a representative speed cell. In the right plot, circle size represents the number of theta cycles. The bottom panel shows median FR (blue) and mean SPC (red) as functions of speed; dashed lines show the linear fit.

(C) Distributions of the slopes of the linear fit between speed and median FR (top) and between speed and mean SPC (middle) for all CA1 speed cells, and their scatterplot (bottom).

neurons not classified as speed cells had a mean lag between firing rate and speed not statistically different from 0 (pyramidal cells: $t(277) = 0.768$, $p = 0.44$; other interneurons: $t(15) = -2.105$, $p = 0.053$), though these cells exhibited a much wider distribution of cross-correlation lag values than the speed cells (Figure S1). In all, we conclude that CA1 speed cells are interneurons and that their firing rate tends to follow—more than lead—changes in locomotion speed.

Pyramidal Cells Are Modulated by Speed but Do Not Encode It

Earlier studies have consistently shown that the firing rate of pyramidal cells increases with speed (McNaughton et al., 1983; Wiener et al., 1989; Czurkó et al., 1999; Hirase et al., 1999; Ekstrom et al., 2001; Maurer et al., 2005). Therefore, at first glance the results above—which indicate that pyramidal cells are not speed cells—seem to be at odds with previous literature. However, it should be noted that here we have measured the correlation between the time series of instantaneous firing rate and locomotion speed, which has recently been used to define speed cells in the medial entorhinal cortex (Kropff et al., 2015). This contrasts with the cited studies that have measured the *average* firing rate of pyramidal cells as a function of speed but have not assessed for firing rate correlations with speed at the timescale of animal behavior.

As shown in Figures 6A and 6B, we were able to reproduce the dependency of the average firing rate of CA1 pyramidal cells on speed when analyzing square arena sessions, thus consistent with previous studies (McNaughton et al., 1983; Wiener et al., 1989; Czurkó et al., 1999; Hirase et al., 1999; Ekstrom et al., 2001; Maurer et al., 2005). However, notice in Figure 6A that while the average firing rate is highly modulated by speed (red lines), no apparent correlation can be inferred from the scatterplots of instantaneous speed versus firing rate (gray dots; compare with the scatterplots of speed cells in Figures 1, 2, and 4). Therefore, while we could confirm that the firing rate of pyramidal cells depends on speed, our results also show that pyramidal cell activity at best only weakly correlates with instantaneous changes in locomotion speed in the open field (Figures 5D, 5E, and 6A).

To further elucidate this matter, we next investigated whether it was possible to decode the time series of animal speed from CA1 neuronal activity using linear decoders (see Kropff et al., 2015 and Method Details). As expected, locomotion speed could be well decoded from the instantaneous firing rate of CA1 units defined as speed cells, and decoding accuracy tended to increase with the number of analyzed speed cells (Figures 6C and 6D; see also Figure S2). On the other hand, locomotion speed in the square open-field arena could not be properly decoded from the instantaneous firing rate of pyramidal cells

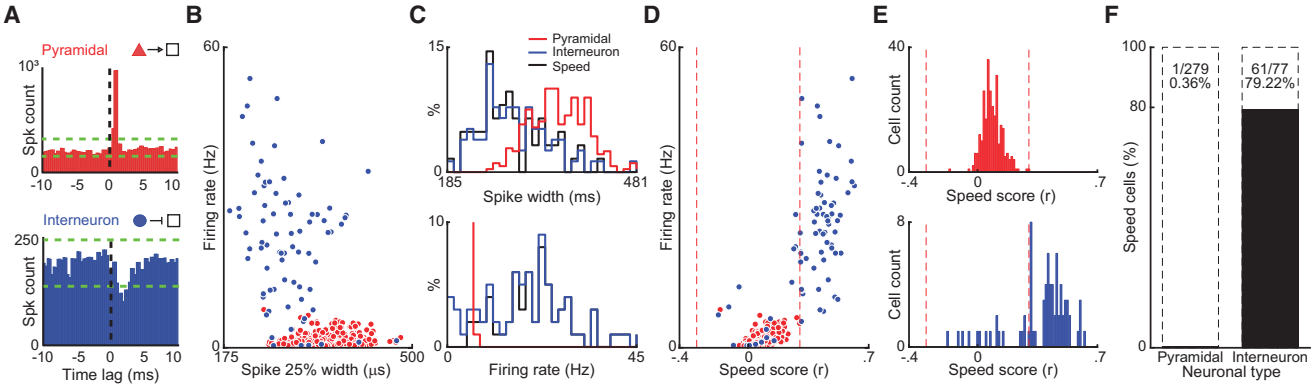

Figure 5. CA1 Speed Cells Are Interneurons

(A) Spike cross-correlograms for reference units (spike at 0) identified as pyramidal cell (top) and interneuron (bottom). Adapted from Mizuseki et al. (2009).

(B) Scatterplot of spike width versus firing rate for pyramidal cells (red) and interneurons (blue).

(C) Distributions of spike width (top) and firing rate (bottom) for pyramidal cells (red), interneurons (blue), and speed cells (black).

(D and E) Scatterplot of speed score versus firing rate (D) and speed score distributions (E) for pyramidal cells (red) and interneurons (blue) recorded in the square open-field arena.

(F) Proportion of speed cells in the square arena among physiologically identified neurons.

(Figure 6C). Accordingly, decoding accuracy was much lower when using the firing rate of pyramidal cells compared to speed cells, irrespective of the number of analyzed cells (Figure 6D). Interestingly, speed cells exhibited higher speed scores and decoded speed better even after down-sampling spikes in such a way as to make them have the same low firing rates as pyramidal cells (Figure 6E). Therefore, despite the increase in average firing rate with speed exhibited by both interneurons and pyramidal cells (Figure 6B; see also Maurer et al., 2005), we conclude that in the open field, only interneurons that are speed cells, but not pyramidal cells, can accurately encode speed at the sub-second timescale.

Pyramidal Cells Spuriously Correlate with Speed in the Linear Track

Figures 1, 2, 3, 4, 5, and 6 showed results for CA1 neurons recorded from animals wandering in the square open-field arena. We next investigated for speed-correlated firing in the linear track. As in the square arena, we found that the majority (64%) of physiologically identified interneurons fulfilled the operational definition of speed cell in the linear track (Figures 7A and 7D, top rows). Moreover, by restricting the analysis to neurons that were recorded within the same day in both the square and linear arenas, we found that 82% of speed cells classified in the square arena were also considered speed cells in the linear track (Figure S3). Therefore, these results indicate that speed coding in the dorsal CA1 is stable across different contexts.

However, we saw a different picture when analyzing the spiking activity of physiologically identified pyramidal cells. While their instantaneous firing rate did not correlate with speed in the square open-field arena (Figures 5 and S1), 35% of the pyramidal cells exhibited speed-correlated firing in the linear track (Figures 7A and 7D). To gain insight into why some pyramidal cells would be considered speed cells only in the linear track but not in the open field, we next investigated their firing rate correlation with speed separately for left and right runs. The motivation for this is that most place cells have unidirectional place fields in the linear track, that is, they exhibit spatial-selective firing only when the animal runs in one of the directions (McNaughton et al., 1983; Muller et al., 1994).

Figure 7B shows a place cell that had a place field during leftward runs (top left panel); also shown is the average animal speed as a function of space for each running direction (bottom left panel). As expected from the nature of this task, the animal's speed stereotypically depended on space, being very low on the edges of the linear track where animals were rewarded and high otherwise. We reasoned that the mutual dependence between speed and space in the linear track might lead to spurious correlations between speed and firing rate for place cells. By spurious we mean that these cells would not genuinely code for speed, and the apparent correlation would instead be due to place fields at locations associated with high locomotion speeds. Consistent with this possibility, notice back in Figure 7A that the example pyramidal cell spiked either at very high and very low rates during high locomotion speeds, which suggests run periods inside and outside the place field, respectively.

If the interdependence between speed and position accounts for the high speed scores observed for some pyramidal cells in the linear track (Figure 7D), the speed-correlated firing should follow spatial coding and be mostly unidirectional. On the other hand, if pyramidal cells truly code for speed, their speed-correlated firing should not depend on running direction. Our further analysis revealed evidence for the first possibility: notice in Figure 7B (right panel) that the average firing rate of the example place cell only increased with speed for the preferred running direction (defined as the direction of highest firing rate). At the group level, we found that pyramidal cells exhibited much higher speed scores for the preferred rather than the non-preferred direction (mean r preferred: 0.270 ± 0.014, non-preferred: 0.065 ± 0.012, $t(322) = 13.5$, $p < 10^{-32}$, paired t test; Figure 7C, bottom), and only 23% of the speed cells defined in the preferred direction were bidirectional. In stark contrast,

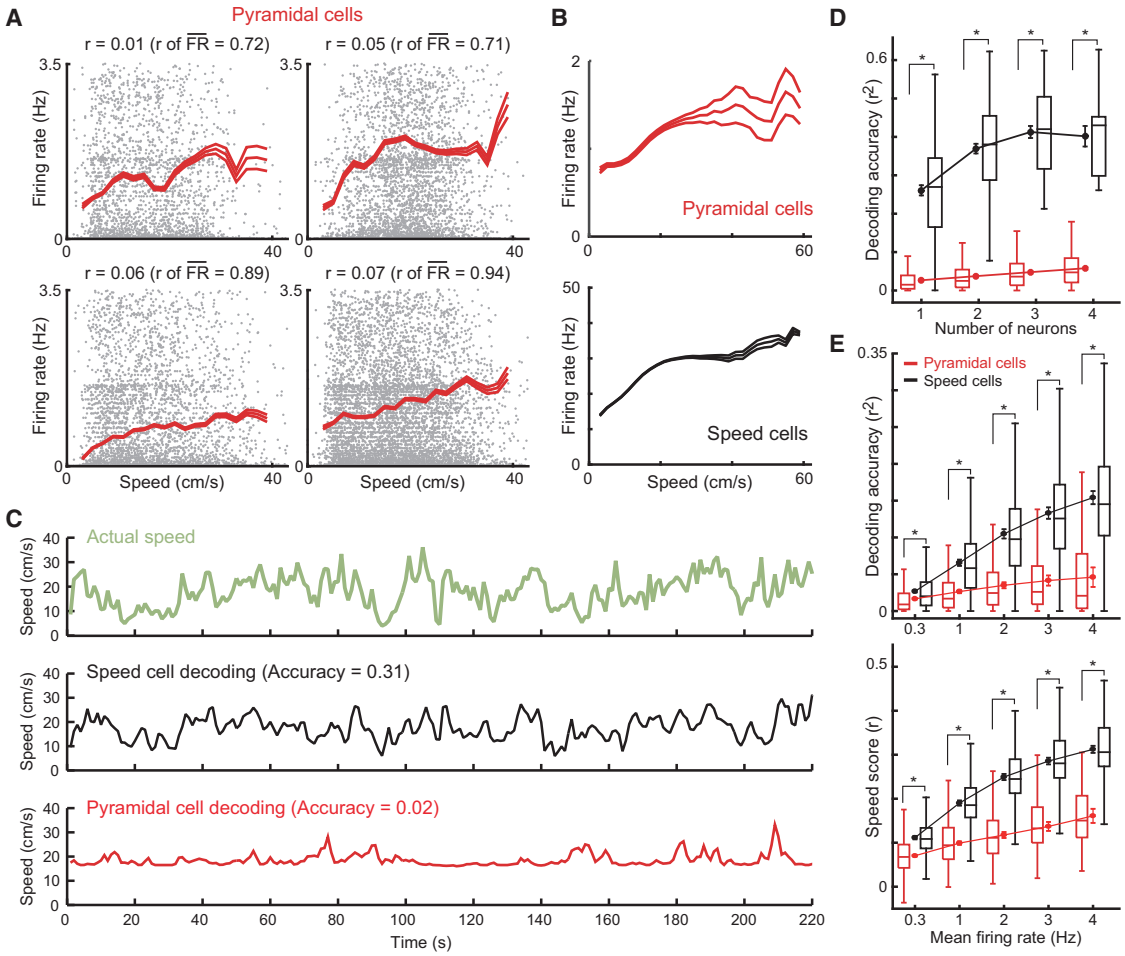

Figure 6. Pyramidal Cells Do Not Encode, but Are Modulated by, Speed

(A) Scatterplots of animal speed versus firing rate (gray dots) for four example pyramidal cells recorded in the square open-field arena. The red lines show the mean firing rate (±SEM). For each panel, the title indicates the speed score (i.e., the correlation coefficient between the instantaneous firing rate and speed) and the correlation coefficient of the mean firing rate ($\overline{FR}$) versus speed.

(B) Group data of mean firing rate (±SEM) as a function of locomotion speed in the open field.

(C) Top panel shows the time series of locomotion speed in the open field. Bottom panels show examples of decoded speed from the firing rate of one speed cell (black) and one pyramidal cell (red).

(D) Boxplot distributions of speed decoding accuracy for pyramidal (red) and speed cells (black) recorded in the square open-field arena. Connected circles show mean ± SEM. Decoding accuracy is defined as the square of the correlation between the decoded and the actual speed time series (i.e., the coefficient of determination). *$p < 0.00001$.

(E) Boxplot distributions of speed scores (bottom) and speed decoding accuracy (top) for individual pyramidal (red) and speed cells (black) after down-sampling spikes to make the two cell types have the same firing rate (see Method Details). Connected circles show mean ± SEM over cells. *$p < 0.00001$.

the speed scores of interneurons did not depend on running direction (mean r preferred: 0.378 ± 0.030, non-preferred: 0.388 ± 0.028, $t(85) = -0.807$, $p = 0.42$, paired t test; Figure 7C, top), and 90% of the speed cells were bidirectional, a statistically significant higher proportion than for pyramidal cells ($\chi^2(1) = 72.94$, $p < 0.00001$).

Our results thus indicate that only interneurons code for speed in the linear track and that the speed-correlated firing of pyramidal cells is spurious and due to the entanglement of speed and position in this task. To further corroborate this conclusion, we next simulated computational models of speed and place cells using real behavioral data from linear and square arena sessions (Figures S4 and S5). In the simulations, the firing rate of the model place cells was solely determined by the instantaneous position of the animal, obtained from real data. Analogously, the firing rate of the model speed cells was solely determined by the instantaneous animal speed. As shown in Figure 7E, simulation results were largely consistent with the conclusion reached above: (1) model speed cells had high speed scores in both open field and linear track simulations; (2) no model place cell correlated with speed in the open field, but half of them were considered speed cells in the linear track even though no speed coding was programmed for these cells (see Figure S5 for simulation results of mixed cell types).

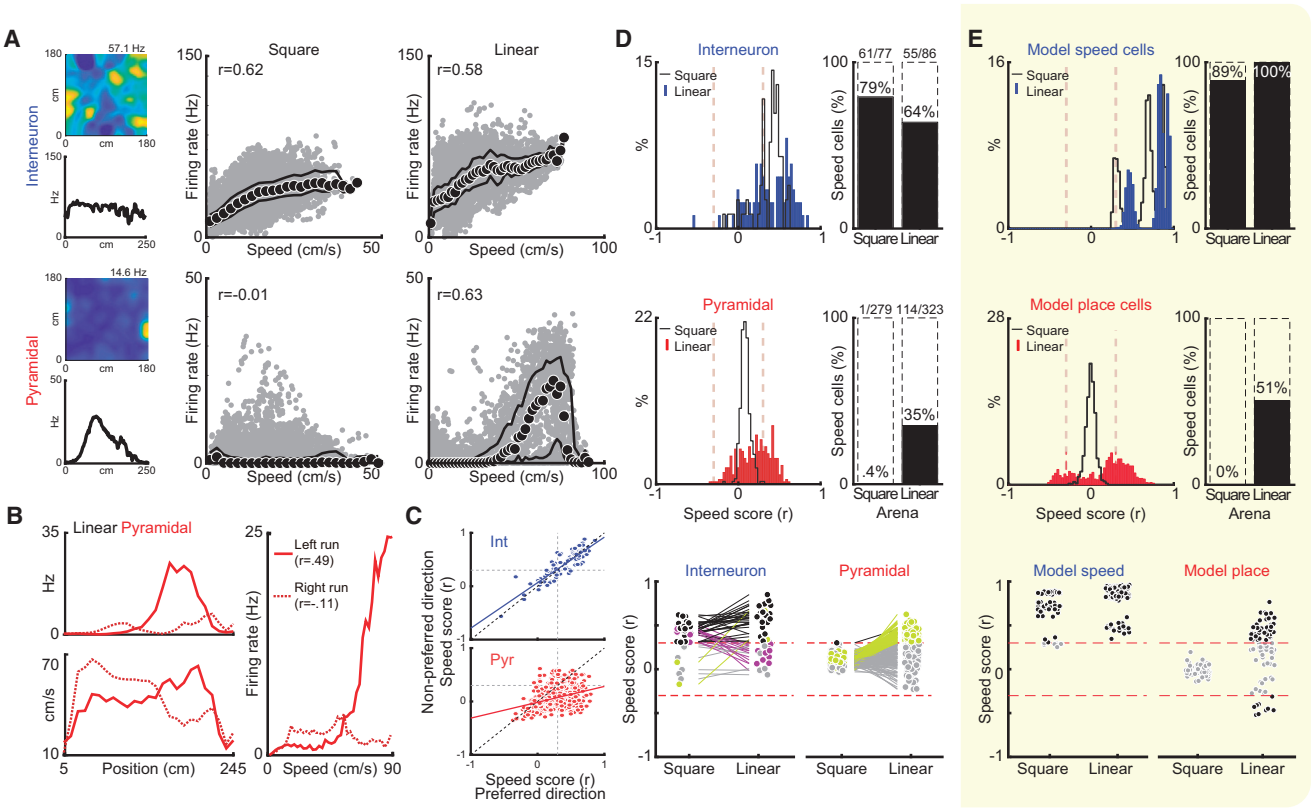

Figure 7. Place Cells Correlate with Speed in Linear Tracks due to the Interdependence of Speed and Position

(A) Left panels show firing rate as a function of space in the square and linear arenas for an interneuron (top) and a pyramidal cell (bottom). Right panels show scatterplots of animal speed versus firing rate for each arena and neuron type. Notice that the instantaneous firing rate of the interneuron correlates with speed in both arenas, while pyramidal cell activity is only correlated with speed in the linear track.

(B) Left panels show mean locomotion speed (bottom) and mean firing rate for a pyramidal cell (top) during left and right runs in the linear track. Right panel shows the mean firing rate during left and right runs as functions of speed.

(C) Scatterplots of speed scores during runs in the preferred (highest firing rate) and non-preferred directions shown separately for interneurons and pyramidal cells. Notice similar scores for interneurons for both run directions (slope: 0.85), while pyramidal cells have much higher speed scores for the preferred direction (slope: 0.29).

(D) Distribution of speed scores and proportion of speed cells among interneurons and pyramidal cells in the square open-field arena ("Square") and in the linear track ("Linear"). Notice high percentage of speed cells among interneurons in both arenas, while around one-third of pyramidal cells are deemed speed cells only in the linear track.

(E) Panels show the same as in (D), but for computational models of place cells and speed cells. Simulations were performed using actual behavioral data (speed and position; see Figure S4). Notice that around half of the simulated place cells are considered speed cells in the linear track, even though these cells did not code for speed by model design.

Finally, we employed a recently described statistical model-based approach (Hardcastle et al., 2017) to infer speed and positional coding by interneurons and pyramidal cells in each arena. Under this framework, the spike train is modeled as a Poisson process of either fixed mean or variable mean dependent on the instantaneous speed and/or position of the animal. In the latter case, the mean rate of the Poisson process is set as the exponential of a linear combination of speed and positional variables (see Method Details), hence these models have been referred to linear-nonlinear-Poisson (LN) models (Hardcastle et al., 2017). Different LN models are used to fit the spiking activity of real neurons, whose coding properties can then be inferred by comparing the log likelihood increase (LLHi) in relation to a Poisson model of fixed firing rate and predictive performance across models (Hardcastle et al., 2017).

We first validated the utility of the LN model approach using simulations of speed and place cell models. Cells were considered to have no coding preference when the LLHis for LN position models and LN speed models were not statistically significantly higher than 0. Otherwise, cells were classified according to the magnitude and significance of the LLHis. As expected, the firing rate of simulated speed cells was better predicted by LN speed models—that is, statistical models whose Poisson rate takes into account the instantaneous speed of the animal (Figure S6). Conversely, simulated place cells were better predicted by LN position models, irrespective of the arena (Figure S6). When applying this statistical approach to real spiking data, most interneurons had a higher LLHi for LN speed models in both the square arena (71%) and linear track (75%), and only 10%–15% displayed a higher LLHi for LN position models;

9%–18% were not significantly modulated by position or speed. In stark contrast, the vast majority of pyramidal cells had a higher LLHi for LN position models in both the square arena (94%) and linear track (88%), while just 6% in either arena did not display coding preference. No pyramidal cell had a higher LLHi for LN speed models in the square arena, and only 6% had a higher LLHi for speed in the linear track. Taking into account all cells irrespective of the significance of the LLHis, in both arenas the percentage of cells whose firing rate was better predicted by speed was high for interneurons (73%) and low for pyramidal cells (0%–9%) (Figure S7). In all, this model-based statistical approach reveals a preferential encoding of speed by interneurons and of space by pyramidal cells, thus consistent with the conclusions reached above through the analysis of correlation coefficients.

DISCUSSION

To the best of our knowledge, we have here performed the most thorough analysis of speed-correlated firing in the dorsal hippocampus to date. Our results show that a subpopulation of hippocampal neurons has a firing rate highly correlated with speed at the sub-second timescale. In line with recent work (Kropff et al., 2015), we referred to these neurons as speed cells. We found that the speed-correlated firing of CA1 speed cells occurs in two different contexts, irrespective of exact position in space and elapsed time. Moreover, the firing rate changes of speed cells tended to follow, more than lead, the changes in locomotion speed. Perhaps of most importance for network models of navigation, our results indicate that the subpopulation of CA1 speed cells is exclusively comprised of inhibitory interneurons. This central conclusion was achieved because (1) virtually no pyramidal cell correlated with speed in the open field arena and (2) the speed-correlated firing of some pyramidal cells in the linear track could be accounted for by spatial coding along with the mutual dependence of animal position and speed in this arena.

At first glance, our main conclusion may seem at odds with numerous reports of firing rate correlations with speed by both pyramidal cells and interneurons (McNaughton et al., 1983; Wiener et al., 1989; O'Keefe et al., 1998; Zhang et al., 1998; Czurkó et al., 1999, 2011; Hirase et al., 1999; Ekstrom et al., 2001; Nitz and McNaughton, 2004; Maurer et al., 2005). A main methodological difference, however, is that we have explored for firing rate correlations with speed at the sub-second scale in which changes in locomotion occur, while previous studies have mostly focused on the average firing rate. Here we were able to reproduce the finding that the average firing rate of both pyramidal cells and interneurons is modulated by speed, even in the open field (Figure 6). However, the speed correlation of the instantaneous firing rate of pyramidal cells was much weaker than that of interneurons, and locomotion speed in the open field could only be reliably decoded from interneurons (Figure 6). In the linear track, we saw a different picture in which the firing rate of 35% of pyramidal cells correlated with speed, but further analysis showed that such correlation could be explained on other grounds than speed coding (Figure 7).

Indeed, when first analyzing the results, it called to our attention that the apparent speed coding by pyramidal cells would occur just in one type of arena (linear track) but not the other (open field) and would depend on running direction. This led us to conclude that it was more parsimonious to ascribe such speed-correlated firing to a by-product of place coding along with the fact that speed and position cannot be disentangled in the linear track due to the nature of the task, which required animals to run back and forth between the end goals. For instance, place cells with place fields in the middle of the track, where the animals display highest speeds in this task, will be considered speed cells by the speed score definition. Consistent with this, computer simulations using the actual behavior of the animal showed that the firing rate of emulated place cells with no programmed speed coding also correlates with speed in the linear track but not in the open field (Figure 7). Moreover, statistical LN models showed that the vast majority of pyramidal cells preferentially encoded position in the linear track, and not speed, with the opposite happening for interneurons (Figure S7).

Although neuronal activity correlated with speed had been previously reported in the medial entorhinal cortex (Sargolini et al., 2006; Wills et al., 2012), speed coding in the hippocampal-entorhinal system has only more recently been better characterized (Hinman et al., 2016; Kropff et al., 2015; Pérez-Escobar et al., 2016; Ye et al., 2018). Namely, Kropff et al. (2015) showed that the medial entorhinal cortex has neurons whose firing rate linearly correlates with speed and called them speed cells, a nomenclature also adopted here (see below for discussion). They further showed that these neurons differed from grid and head direction cells, suggesting a functionally dedicated group (but see Hardcastle et al., 2017), and that they were stable across contexts. Importantly, Kropff et al. (2015) have also reported cells with similar characteristics in the hippocampus. Further consistent with our results, in a recent follow-up study, the same group reported that a large proportion of entorhinal cortex speed cells are fast-spiking interneurons (Ye et al., 2018; see also Pérez-Escobar et al., 2016). Moreover, they showed that a subset of speed-modulated GABAergic neurons project directly to the hippocampus (Ye et al., 2018). Interestingly, a main difference between the two regions is that the hippocampal speed cells better correlate with immediate past speeds (−65 ms; Figure S1; see also Kropff et al., 2015), while speed cells in the entorhinal cortex display prospective coding—that is, their firing rate correlates better with immediate future speeds (+60 ms; Kropff et al., 2015). These findings, however, should be interpreted with care since the video frames were acquired with a temporal resolution of 33–20 ms (30–50 Hz fps).

It is worth noticing that we have used a much more conservative threshold for defining speed cells ($|r| > 0.3$) than the one based on surrogate data used in recent studies (Kropff et al., 2015; Pérez-Escobar et al., 2016; Ye et al., 2018). This more stringent threshold was motivated by the verification of a clear bimodal distribution of speed scores, which would not be well separated by the surrogate-based threshold (Figure 3). Moreover, excitatory cells of the entorhinal-hippocampal system have weak but positive correlations with speed (Figure 5E; Ye et al., 2018), likely because they are most active during traversals of their spatial receptive field, thus causing a positive bias for higher activity during locomotion. We believe the use of less conservative thresholds may account for the inclusion of excitatory

cells in the population of speed cells in the entorhinal cortex studies (Kropff et al., 2015; Pérez-Escobar et al., 2016; Ye et al., 2018).

The definition of neuronal encoding is often linked to the capacity of decoding information from neuronal activity (i.e., to neuronal decoding). That is, in practice, a neuron is considered to encode information about a given feature if it is possible to retrieve this information from the analysis of its spike train (Bialek et al., 1991; Quian Quiroga and Panzeri, 2009; Rieke, 1999; Rolls and Treves, 2011; Stanley, 2013). In this sense, the present work employed the same operational definition as in most of the current neuroscience research: since animal speed could be successfully decoded from the firing rate of hippocampal speed cells, these cells were interpreted as encoding information about speed. However, it may be too simplistic to assume that a value-encoding process takes place solely based on correlations between external variables and neuronal activity (Wiener et al., 1989). Instead of encoding the scalar value of speed, the hippocampal interneurons may be only modulated by speed. Judging whether information is value encoded also depends on knowing how such a code—if existent—is read by downstream neurons, a challenging and seldom tackled question in neuroscience (Buzsáki, 2010; Stanley, 2013). Thus, as long as neuronal coding and decoding are dual definitions, it is impossible to operationally separate encoding from modulated activity, and the natural question as to whether inhibitory interneurons provide an actual speed signal is at present difficult to solve. In any case, it is clear that speed does affect local networks through the activity of interneurons.

We also note that the nomenclature employed here and in other recent studies—namely of calling neurons whose instantaneous firing rate has high correlation with speed as speed cells—may not be the most appropriate one. We opted to use this notation for the sake of convenience; clearly, speed cells reads much faster than "neurons whose firing rate correlates with speed." But aside from the convenience of notation, we do not mean to imply that speed cells only code (if they code) for speed. For instance, we here showed that hippocampal speed cells are interneurons, and, in fact, speed modulates a large proportion of local GABAergic cells (Figure 5). Inhibitory interneurons are well known to have several functions, such as control of input and output activity of pyramidal cells, generation of oscillatory activity, and segregation of cell assembly sequences (Freund and Buzsáki, 1996; Klausberger and Somogyi, 2008; Pelkey et al., 2017). Thus, the speed cells certainly play many more roles in addition to conveying speed-modulated inhibition to the local network. Of note, similar terminology has been previously employed for other types of neurons, such as "place cells," which are known to code for much more than only position (Aronov et al., 2017; Eichenbaum, 2000; Wood et al., 2000).

Neurons of the hippocampal formation have been previously linked to both allocentric- and egocentric-based spatial navigation (Buzsáki and Moser, 2013; Hartley et al., 2014; Moser et al., 2008). Theoretically, path integration can be achieved from the knowledge of the initial position, locomotion direction, and traveled distance (McNaughton et al., 2006). To estimate the latter, speed must be integrated over elapsed time. Accordingly, models of path integration assume the existence of a speed signal impinging on specific neurons (Burak and Fiete, 2009; Couey et al., 2013; Fuhs and Touretzky, 2006; McNaughton et al., 2006; Navratilova et al., 2012). While the sparse spiking of pyramidal cells would make them well suited for position coding, the high firing rates of GABAergic interneurons may be instantaneously adjusted according to locomotion speed and would thus provide the required signal to the network. Interestingly, we found that speed cells decode speed better than pyramidal cells even after controlling for differences in firing rate (Figure 6E), likely because interneurons tend to be active all over the arena. Of note, the CA1 speed cells were not modulated by movement direction (not shown). Therefore, for speed cells to play a role in path integration, the speed information conveyed by them should be combined with the directional information provided by head-direction cells. Under this scenario, path integration would not be a function of a unique cell type but would require downstream reader neurons to integrate multiple sources of information.

Our results are consistent with a recent computational model of phase precession (Chadwick et al., 2016). This model was able to account for the speed dependence of the rate of change in the spiking theta phase of place cells as the animal traverses the place field, in which the temporal slope of phase precession is steeper for faster speeds. In turn, the variable temporal slope allows for a fixed relation between spiking theta phase and position at different running speeds (Huxter et al., 2003; Geisler et al., 2007). The model results crucially relied on the activity of interneurons, which were predicted to receive excitatory inputs dependent on speed (Chadwick et al., 2016). Consistent with this possibility, glutamatergic cells of the medial septum were recently shown to provide CA1 interneurons with a depolarizing drive that increases with running speed (Fuhrmann et al., 2015). Neurons modulated by speed in other subcortical structures such as the mammillary bodies, habenula, and interpeduncular nucleus could potentially contribute (Sharp and Turner-Williams, 2005; Sharp et al., 2006). Regardless of the source of excitation, by demonstrating their high modulation by speed, our results support the idea that the activity of inhibitory interneurons in CA1 would allow for flexible timescales of theta spiking sequences (Chadwick et al., 2016).

On average, pyramidal cells spiked more with running speed (Figure 6). This result is seemingly discrepant with the positive speed correlation exhibited by most speed cells (Figures 3 and 5), which are interneurons and should thus inhibit pyramidal cells at higher speeds. Possible solutions to this conundrum include network scenarios in which (1) both interneurons and pyramidal cells receive a common, speed-dependent excitatory drive, (2) the firing rate of interneurons is primarily determined by the activity of pyramidal cells at the population level (which would provide a higher net excitation with higher speeds), or (3) synaptic connections among inhibitory interneurons lead to a disinhibition of pyramidal cells. Evidence for the latter scenario has been reported by Fuhrmann et al. (2015), who showed that interneurons located in stratum oriens and alveus, such as oriens-lacunosum moleculare (OLM) cells, are excited by septal glutamatergic neurons and in turn inhibit interneurons in stratum radiatum and stratum lacunosum-moleculare that mediate feed-forward inhibition onto pyramidal cells. However, the recordings analyzed here targeted the pyramidal cell layer, and it is thus

likely that the speed cells also comprised fast-spiking, parvalbumin-positive basket cells that provide perisomatic inhibition. Actually, since a high percentage of interneurons were classified as speed cells (Figures 5, 7, S1, and S7), we believe the CA1 speed cell population included multiple interneuron subtypes. This is consistent with the fact that the preferred spiking theta phase varied among speed cells (Figure S1).

Our findings are also consistent with a recent study in awake head-fixed mice that tracked neuronal activity through Ca^{+2} imaging (Arriaga and Han, 2017). They found that Ca^{+2} fluctuations of most interneurons (>74%) were positively correlated with speed while the animals navigated in a virtual environment and that speed modulated both parvalbumin- and somatostatin-positive interneurons located in different hippocampal layers, which is to say that speed modulated different morphological subtypes of interneurons. Interestingly, the fluorescence signals were anti-correlated with speed for ~14%–18% of cells (Arriaga and Han, 2017), a higher percentage than the 8.6% of "negative" speed cells found here (8/93; Figure 3). Also similar to our findings, the imaging results showed that the speed correlations of Ca^{+2} fluctuations were stable over time and different virtual environments.

In summary, we have shown that inhibitory interneurons, and not pyramidal cells, are likely to convey a reliable rate-coded speed signal to the hippocampus, which is stable across contexts, position in space, and elapsed time. This finding should shed new light on network models of spatial navigation.

STAR★METHODS

Detailed methods are provided in the online version of this paper and include the following:

- KEY RESOURCES TABLE
- CONTACT FOR REAGENT AND RESOURCE SHARING
- EXPERIMENTAL MODEL AND SUBJECT DETAILS
- METHOD DETAILS
  - Microdrive implantation
  - Spatial arenas
  - Data acquisition
  - Spike detection and sorting
  - Recording selection
  - Speed score and speed cell definitions
  - Scatterplots of speed versus firing rate
  - Spatial heatmaps
  - Analysis of speed cell stability across space and time
  - Speed-binned autocorrelogram
  - Spike count per theta cycle
  - Neuron type classification
  - Linear decoders
  - Computational models of place and speed cells
  - Linear-nonlinear algorithm
- QUANTIFICATION AND STATISTICAL ANALYSIS
- DATA AND SOFTWARE AVAILABILITY

SUPPLEMENTAL INFORMATION

Supplemental Information includes seven figures and can be found with this article online at https://doi.org/10.1016/j.celrep.2018.10.054.

ACKNOWLEDGMENTS

Supported by Conselho Nacional de Desenvolvimento Científico e Tecnológico (CNPq) and Coordenação de Aperfeiçoamento de Pessoal de Nível Superior (CAPES). The authors thank the Buzsáki laboratory for making data publicly available at http://crcns.org/, a data-sharing website supported by NSF and NIH, USA. The authors also thank Kiah Hardcastle, Niru Maheswaranathan, and the Giocomo laboratory for making LN-model codes publicly available at https://github.com/GiocomoLab/.

AUTHOR CONTRIBUTIONS

A.B.L.T. designed research; Z.H.T.D.G. analyzed data; A.B.L.T. and Z.H.T.D.G. wrote the manuscript.

DECLARATION OF INTERESTS

The authors declare no competing interests.

Received: June 6, 2018
Revised: August 15, 2018
Accepted: October 12, 2018
Published: November 13, 2018

REFERENCES

Aronov, D., Nevers, R., and Tank, D.W. (2017). Mapping of a non-spatial dimension by the hippocampal-entorhinal circuit. Nature *543*, 719–722.

Arriaga, M., and Han, E.B. (2017). Dedicated hippocampal inhibitory networks for locomotion and immobility. J. Neurosci. *37*, 9222–9238.

Bialek, W., Rieke, F., de Ruyter van Steveninck, R.R., and Warland, D. (1991). Reading a neural code. Science *252*, 1854–1857.

Buckner, R.L. (2010). The role of the hippocampus in prediction and imagination. Annu. Rev. Psychol. *61*, 27–48.

Burak, Y., and Fiete, I.R. (2009). Accurate path integration in continuous attractor network models of grid cells. PLoS Comput. Biol. *5*, e1000291.

Buzsáki, G. (2002). Theta oscillations in the hippocampus. Neuron *33*, 325–340.

Buzsáki, G. (2005). Theta rhythm of navigation: link between path integration and landmark navigation, episodic and semantic memory. Hippocampus *15*, 827–840.

Buzsáki, G. (2010). Neural syntax: cell assemblies, synapsembles, and readers. Neuron *68*, 362–385.

Buzsáki, G., and Moser, E.I. (2013). Memory, navigation and theta rhythm in the hippocampal-entorhinal system. Nat. Neurosci. *16*, 130–138.

Chadwick, A., van Rossum, M.C., and Nolan, M.F. (2016). Flexible theta sequence compression mediated via phase precessing interneurons. eLife *5*, e20349.

Couey, J.J., Witoelar, A., Zhang, S.-J., Zheng, K., Ye, J., Dunn, B., Czajkowski, R., Moser, M.-B., Moser, E.I., Roudi, Y., and Witter, M.P. (2013). Recurrent inhibitory circuitry as a mechanism for grid formation. Nat. Neurosci. *16*, 318–324.

Csicsvari, J., Hirase, H., Czurkó, A., Mamiya, A., and Buzsáki, G. (1999). Oscillatory coupling of hippocampal pyramidal cells and interneurons in the behaving Rat. J. Neurosci. *19*, 274–287.

Czurkó, A., Hirase, H., Csicsvari, J., and Buzsáki, G. (1999). Sustained activation of hippocampal pyramidal cells by 'space clamping' in a running wheel. Eur. J. Neurosci. *11*, 344–352.

Czurkó, A., Huxter, J., Li, Y., Hangya, B., and Muller, R.U. (2011). Theta phase classification of interneurons in the hippocampal formation of freely moving rats. J. Neurosci. *31*, 2938–2947.

Diba, K., and Buzsáki, G. (2008). Hippocampal network dynamics constrain the time lag between pyramidal cells across modified environments. J. Neurosci. *28*, 13448–13456.

Dragoi, G., and Buzsáki, G. (2006). Temporal encoding of place sequences by hippocampal cell assemblies. Neuron *50*, 145–157.

Eichenbaum, H. (2000). Hippocampus: mapping or memory? Curr. Biol. *10*, R785–R787.

Ekstrom, A.D., Meltzer, J., McNaughton, B.L., and Barnes, C.A. (2001). NMDA receptor antagonism blocks experience-dependent expansion of hippocampal "place fields". Neuron *31*, 631–638.

Ferbinteanu, J., and Shapiro, M.L. (2003). Prospective and retrospective memory coding in the hippocampus. Neuron *40*, 1227–1239.

Frank, L.M., Brown, E.N., and Wilson, M.A. (2001). A comparison of the firing properties of putative excitatory and inhibitory neurons from CA1 and the entorhinal cortex. J. Neurophysiol. *86*, 2029–2040.

Freund, T.F., and Buzsáki, G. (1996). Interneurons of the hippocampus. Hippocampus *6*, 347–470.

Fuhrmann, F., Justus, D., Sosulina, L., Kaneko, H., Beutel, T., Friedrichs, D., Schoch, S., Schwarz, M.K., Fuhrmann, M., and Remy, S. (2015). Locomotion, theta oscillations, and the speed-correlated firing of hippocampal neurons are controlled by a medial septal glutamatergic circuit. Neuron *86*, 1253–1264.

Fuhs, M.C., and Touretzky, D.S. (2006). A spin glass model of path integration in rat medial entorhinal cortex. J. Neurosci. *26*, 4266–4276.

Fujisawa, S., Amarasingham, A., Harrison, M.T., and Buzsáki, G. (2008). Behavior-dependent short-term assembly dynamics in the medial prefrontal cortex. Nat. Neurosci. *11*, 823–833.

Geisler, C., Robbe, D., Zugaro, M., Sirota, A., and Buzsáki, G. (2007). Hippocampal place cell assemblies are speed-controlled oscillators. Proc. Natl. Acad. Sci. USA *104*, 8149–8154.

Grieves, R.M., and Jeffery, K.J. (2017). The representation of space in the brain. Behav. Processes *135*, 113–131.

Hafting, T., Fyhn, M., Molden, S., Moser, M.-B., and Moser, E.I. (2005). Microstructure of a spatial map in the entorhinal cortex. Nature *436*, 801–806.

Hardcastle, K., Maheswaranathan, N., Ganguli, S., and Giocomo, L.M. (2017). A multiplexed, heterogeneous, and adaptive code for navigation in medial entorhinal cortex. Neuron *94*, 375–387.e7.

Harris, K.D., Henze, D.A., Csicsvari, J., Hirase, H., and Buzsáki, G. (2000). Accuracy of tetrode spike separation as determined by simultaneous intracellular and extracellular measurements. J. Neurophysiol. *84*, 401–414.

Hartley, T., Lever, C., Burgess, N., and O'Keefe, J. (2014). Space in the brain: how the hippocampal formation supports spatial cognition. Philos. Trans. R. Soc. Lond. B Biol. Sci. *369*, 20120510.

Hazan, L., Zugaro, M., and Buzsáki, G. (2006). Klusters, NeuroScope, NDManager: a free software suite for neurophysiological data processing and visualization. J. Neurosci. Methods *155*, 207–216.

Hinman, J.R., Penley, S.C., Long, L.L., Escabí, M.A., and Chrobak, J.J. (2011). Septotemporal variation in dynamics of theta: speed and habituation. J. Neurophysiol. *105*, 2675–2686.

Hinman, J.R., Brandon, M.P., Climer, J.R., Chapman, G.W., and Hasselmo, M.E. (2016). Multiple running speed signals in medial entorhinal cortex. Neuron *91*, 666–679.

Hirase, H., Czurkó, A., Csicsvari, J., and Buzsáki, G. (1999). Firing rate and theta-phase coding by hippocampal pyramidal neurons during 'space clamping'. Eur. J. Neurosci. *11*, 4373–4380.

Huxter, J., Burgess, N., and O'Keefe, J. (2003). Independent rate and temporal coding in hippocampal pyramidal cells. Nature *425*, 828–832.

Klausberger, T., and Somogyi, P. (2008). Neuronal diversity and temporal dynamics: the unity of hippocampal circuit operations. Science *321*, 53–57.

Klausberger, T., Magill, P.J., Márton, L.F., Roberts, J.D.B., Cobden, P.M., Buzsáki, G., and Somogyi, P. (2003). Brain-state- and cell-type-specific firing of hippocampal interneurons in vivo. Nature *421*, 844–848.

Knierim, J.J., Kudrimoti, H.S., and McNaughton, B.L. (1998). Interactions between idiothetic cues and external landmarks in the control of place cells and head direction cells. J. Neurophysiol. *80*, 425–446.

Kropff, E., Carmichael, J.E., Moser, M.-B., and Moser, E.I. (2015). Speed cells in the medial entorhinal cortex. Nature *523*, 419–424.

Lever, C., Cacucci, F., Wills, T., Burton, S., McClelland, A., Burgess, N., and O'Keefe, J. (2003). Spatial coding in the hippocampal formation: input, information type, plasticity and behaviour. In The Neurobiology of Spatial Behaviour, K.J. Jeffery, ed. (Oxford University Press), pp. 199–225.

Maurer, A.P., Vanrhoads, S.R., Sutherland, G.R., Lipa, P., and McNaughton, B.L. (2005). Self-motion and the origin of differential spatial scaling along the septo-temporal axis of the hippocampus. Hippocampus *15*, 841–852.

McNaughton, B.L., Barnes, C.A., and O'Keefe, J. (1983). The contributions of position, direction, and velocity to single unit activity in the hippocampus of freely-moving rats. Exp. Brain Res. *52*, 41–49.

McNaughton, B.L., Leonard, B., and Chen, L. (1989). Cortical-hippocampal interactions and cognitive mapping: a hypothesis based on reintegration of the parietal and inferotemporal pathways for visual processing. Psychobiology *17*, 230–235.

McNaughton, B.L., Barnes, C.A., Gerrard, J.L., Gothard, K., Jung, M.W., Knierim, J.J., Kudrimoti, H., Qin, Y., Skaggs, W.E., Suster, M., and Weaver, K.L. (1996). Deciphering the hippocampal polyglot: the hippocampus as a path integration system. J. Exp. Biol. *199*, 173–185.

McNaughton, B.L., Battaglia, F.P., Jensen, O., Moser, E.I., and Moser, M.-B. (2006). Path integration and the neural basis of the 'cognitive map'. Nat. Rev. Neurosci. *7*, 663–678.

Mizuseki, K., Sirota, A., Pastalkova, E., and Buzsáki, G. (2009). Theta oscillations provide temporal windows for local circuit computation in the entorhinal-hippocampal loop. Neuron *64*, 267–280.

Mizuseki, K., Sirota, A., Pastalkova, E., Diba, K., and Buzsáki, G. (2013). Multiple single unit recordings from different rat hippocampal and entorhinal regions while the animals were performing multiple behavioral tasks (CRCNS Org).

Mizuseki, K., Diba, K., Pastalkova, E., Teeters, J., Sirota, A., and Buzsáki, G. (2014). Neurosharing: large-scale data sets (spike, LFP) recorded from the hippocampal-entorhinal system in behaving rats. F1000Res. *3*, 98.

Moser, E.I., Kropff, E., and Moser, M.-B. (2008). Place cells, grid cells, and the brain's spatial representation system. Annu. Rev. Neurosci. *31*, 69–89.

Muller, R.U., and Kubie, J.L. (1987). The effects of changes in the environment on the spatial firing of hippocampal complex-spike cells. J. Neurosci. *7*, 1951–1968.

Muller, R.U., Bostock, E., Taube, J.S., and Kubie, J.L. (1994). On the directional firing properties of hippocampal place cells. J. Neurosci. *14*, 7235–7251.

Navratilova, Z., Giocomo, L.M., Fellous, J.-M., Hasselmo, M.E., and McNaughton, B.L. (2012). Phase precession and variable spatial scaling in a periodic attractor map model of medial entorhinal grid cells with realistic after-spike dynamics. Hippocampus *22*, 772–789.

Nitz, D., and McNaughton, B. (2004). Differential modulation of CA1 and dentate gyrus interneurons during exploration of novel environments. J. Neurophysiol. *91*, 863–872.

O'Keefe, J. (1976). Place units in the hippocampus of the freely moving rat. Exp. Neurol. *51*, 78–109.

O'Keefe, J., and Conway, D.H. (1978). Hippocampal place units in the freely moving rat: why they fire where they fire. Exp. Brain Res. *31*, 573–590.

O'Keefe, J., and Dostrovsky, J. (1971). The hippocampus as a spatial map. Preliminary evidence from unit activity in the freely-moving rat. Brain Res. *34*, 171–175.

O'Keefe, J., and Speakman, A. (1987). Single unit activity in the rat hippocampus during a spatial memory task. Exp. Brain Res. *68*, 1–27.

O'Keefe, J., Burgess, N., Donnett, J.G., Jeffery, K.J., and Maguire, E.A. (1998). Place cells, navigational accuracy, and the human hippocampus. Philos. Trans. R. Soc. Lond. B Biol. Sci. *353*, 1333–1340.

Pelkey, K.A., Chittajallu, R., Craig, M.T., Tricoire, L., Wester, J.C., and McBain, C.J. (2017). Hippocampal GABAergic inhibitory interneurons. Physiol. Rev. *97*, 1619–1747.

Pérez-Escobar, J.A., Kornienko, O., Latuske, P., Kohler, L., and Allen, K. (2016). Visual landmarks sharpen grid cell metric and confer context specificity to neurons of the medial entorhinal cortex. eLife *5*, e16937.

Quian Quiroga, R., and Panzeri, S. (2009). Extracting information from neuronal populations: information theory and decoding approaches. Nat. Rev. Neurosci. *10*, 173–185.

Quirk, G.J., Muller, R.U., and Kubie, J.L. (1990). The firing of hippocampal place cells in the dark depends on the rat's recent experience. J. Neurosci. *10*, 2008–2017.

Rieke, F. (1999). Spikes: Exploring the Neural Code (MIT Press).

Rolls, E.T., and Treves, A. (2011). The neuronal encoding of information in the brain. Prog. Neurobiol. *95*, 448–490.

Sanders, H., Rennó-Costa, C., Idiart, M., and Lisman, J. (2015). Grid cells and place cells: an integrated view of their navigational and memory function. Trends Neurosci. *38*, 763–775.

Sargolini, F., Fyhn, M., Hafting, T., McNaughton, B.L., Witter, M.P., Moser, M.-B., and Moser, E.I. (2006). Conjunctive representation of position, direction, and velocity in entorhinal cortex. Science *312*, 758–762.

Sharp, P.E., and Turner-Williams, S. (2005). Movement-related correlates of single-cell activity in the medial mammillary nucleus of the rat during a pellet-chasing task. J. Neurophysiol. *94*, 1920–1927.

Sharp, P.E., Kubie, J.L., and Muller, R.U. (1990). Firing properties of hippocampal neurons in a visually symmetrical environment: contributions of multiple sensory cues and mnemonic processes. J. Neurosci. *10*, 3093–3105.

Sharp, P.E., Turner-Williams, S., and Tuttle, S. (2006). Movement-related correlates of single cell activity in the interpeduncular nucleus and habenula of the rat during a pellet-chasing task. Behav. Brain Res. *166*, 55–70.

Sirota, A., Montgomery, S., Fujisawa, S., Isomura, Y., Zugaro, M., and Buzsáki, G. (2008). Entrainment of neocortical neurons and gamma oscillations by the hippocampal theta rhythm. Neuron *60*, 683–697.

Sławińska, U., and Kasicki, S. (1998). The frequency of rat's hippocampal theta rhythm is related to the speed of locomotion. Brain Res. *796*, 327–331.

Stanley, G.B. (2013). Reading and writing the neural code. Nat. Neurosci. *16*, 259–263.

Taube, J.S., Muller, R.U., and Ranck, J.B., Jr. (1990). Head-direction cells recorded from the postsubiculum in freely moving rats. I. Description and quantitative analysis. J. Neurosci. *10*, 420–435.

Whishaw, I.Q. (1998). Place learning in hippocampal rats and the path integration hypothesis. Neurosci. Biobehav. Rev. *22*, 209–220.

Whishaw, I.Q., and Brooks, B.L. (1999). Calibrating space: exploration is important for allothetic and idiothetic navigation. Hippocampus *9*, 659–667.

Wiener, S.I., Paul, C.A., and Eichenbaum, H. (1989). Spatial and behavioral correlates of hippocampal neuronal activity. J. Neurosci. *9*, 2737–2763.

Wills, T.J., Barry, C., and Cacucci, F. (2012). The abrupt development of adult-like grid cell firing in the medial entorhinal cortex. Front. Neural Circuits *6*, 21.

Wood, E.R., Dudchenko, P.A., Robitsek, R.J., and Eichenbaum, H. (2000). Hippocampal neurons encode information about different types of memory episodes occurring in the same location. Neuron *27*, 623–633.

Ye, J., Witter, M.P., Moser, M.-B., and Moser, E.I. (2018). Entorhinal fast-spiking speed cells project to the hippocampus. Proc. Natl. Acad. Sci. USA *115*, E1627–E1636.

Zhang, K., Ginzburg, I., McNaughton, B.L., and Sejnowski, T.J. (1998). Interpreting neuronal population activity by reconstruction: unified framework with application to hippocampal place cells. J. Neurophysiol. *79*, 1017–1044.

STAR★METHODS

KEY RESOURCES TABLE

REAGENT or RESOURCE	SOURCE	IDENTIFIER
Deposited Data		
HC3 Dataset	CRCNS	http://crcns.org/data-sets/hc/hc-3
Software and Algorithms		
MATLAB	Mathworks	https://www.mathworks.com/
LN model MATLAB codes	Giocomo Lab; Hardcastle et al., 2017	https://github.com/GiocomoLab/ln-model-of-mec-neurons/

CONTACT FOR REAGENT AND RESOURCE SHARING

Further information and requests for resources and reagents should be directed to and will be fulfilled by the Lead Contact, Adriano Tort (tort@neuro.ufrn.br).

EXPERIMENTAL MODEL AND SUBJECT DETAILS

Data from three male Long-Evans rats (250-400 g) were analyzed. The experiments were approved by the Institutional Animal Care and Use Committee of Rutgers University.

METHOD DETAILS

We analyzed recordings of hippocampal neuronal activity generously made available by the Buzsáki laboratory through the Collaborative Research in Computational Neuroscience data sharing website (http://crcns.org, hc-3 dataset). Detailed descriptions of the experimental procedures can be found in previous publications (Diba and Buzsáki, 2008; Mizuseki et al., 2009, 2013, 2014). All protocols were approved by the Institutional Animal Care and Use Committee of Rutgers University. Below we describe the analytical methods employed by us, and, for convenience, also the relevant experimental procedures from the original publications (microdrive implantation, spatial arenas, data acquisition, spike detection and sorting, and neuron type classification).

Microdrive implantation

Three male Long-Evans rats (250-400 g) were implanted with a 4- or 8-shank silicon probe (200-μm inter-shank distance) attached to a microdrive in the right dorsal hippocampus. Each shank had 8 recording sites (160 μm^2 each site; 1-3 MΩ impedance). Shanks were aligned parallel to the septotemporal axis (angled at 45° parasagittal), and centrally positioned at $-$3.5 mm AP and 2.5 mm ML. Two stainless steel screws implanted above the cerebellum served as indifferent and ground electrodes. Shank positioning was verified histologically.

Spatial arenas

We selected from the hc-3 dataset all rats that (1) had CA1 units and (2) were recorded in both the square and linear arenas. Accordingly, we analyzed CA1 activity from three rats (ec013, ec014, ec016) over 163 sessions: 62 sessions were recorded in a 180-cm sided square arena (“bigSquare”; 45, 4 and 13 sessions for each rat, respectively), and 101 sessions in an elevated 250-cm x 7-cm linear arena (“linear”; 90, 2 and 9 sessions, respectively). In the square open-field arena, animals chased for randomly dispersed drops of water or pieces of Froot Loops ($\sim$25 mg Kellogg’s); in the linear arena, animals ran back and forth for 30 μL water reward on both ends.

Data acquisition

Neuroelectrophysiological recordings were performed using a 128-channel DataMax system (16-bit resolution; RC Electronics). Signals were amplified (1,000 X), filtered between 1 and 5,000 Hz, and acquired continuously at 20,000 Hz. Local field potentials (LFPs) were obtained by decimating original signal to 1,250 Hz. Animal behavior was video-recorded through a camera mounted on the top of the arena (30 frames per second). The animal position was tracked from the XY coordinates of two light-emitting diodes on the headstage and was interpolated to 39.0625 Hz.

Spike detection and sorting

The original signal was filtered between 800 and 5,000 Hz and its root mean square (RMS) was computed. Spike detection threshold was defined as five times the standard deviation from the mean RMS over sliding windows of 0.2 ms. Waveforms were interpolated to

40,000 Hz and semi-automatically sorted by first using KlustaKwik software (http://klustakwik.sourceforge.net; Harris et al., 2000), followed by manual adjustment of neuron clusters using Klusters software (http://klusters.sourceforge.net; Hazan et al., 2006). Only clusters with clear boundaries and refractory periods were considered as single units. Neuronal waveforms recorded on different days were clustered separately.

Recording selection

For neurons with multiple recordings in the same arena (i.e., "linear" or "bigSquare"), we selected the recording session in which the neuron elicited the highest number of spikes.

Speed score and speed cell definitions

The instantaneous animal speed was computed as the displacement of the animal tracking between two consecutive frames divided by the inter-frame interval (25.6 ms). The speed time-series was obtained by smoothing the instantaneous animal speed with a 1D-Gaussian with 250-ms standard deviation. The firing rate time series was obtained by smoothing spike counts over inter-frame intervals with the same Gaussian. The speed score of a neuron was defined as the Pearson's product-moment correlation coefficient (Pearson's r) between the time series of its firing rate and animal speed. In Figure 3, surrogate speed scores were obtained by computing the Pearson's r between animal speed and the firing rate time series randomly circularly shifted between ± 90 s. Speed cells were operationally defined as neurons whose absolute speed score for the square arena was greater than 0.3. We opted to use this operational definition, which is more conservative than a surrogate-based threshold, because (1) the bimodality in the distribution of observed speed scores can be separated at 0.3 (see Figure 3A), and (2) a surrogate-based threshold (e.g., 4 SD from the surrogate mean) would give rise to speed cells with very low speed scores, which likely correspond to a by-product of place-field firing.

Scatterplots of speed versus firing rate

For the sake of visibility, the gray dots in the scatterplots of speed versus firing rate shown in Figures 1D, 2C, S3A, S3B, and 4B depict only 10% of the data, selected at random. The black circles and lines display the quantiles 25, 50 and 75 computed using all data within overlapping speed bins (bin width = 6 cm/s, bin step = 2 cm/s).

Spatial heatmaps

We constructed heatmaps to visualize the spatial distribution of (1) animal time occupancy, (2) animal speed and (3) neuronal firing rate. To that end, for each heatmap we summed 2D-Gaussians with 5-cm standard deviation centered in the XY tracking coordinates with volumes equal to the (1) inter-frame interval, (2) animal speed or (3) firing rate associated to each tracking sample. The heatmaps were plotted using 100 × 100 bins.

Analysis of speed cell stability across space and time

To assess if speed coding by firing rate is stable across space, in Figures 2C and 3D we computed speed scores using only data for when the animal was within a specific subregion of the square arena: either in each of its four quadrants (90 cm x 90 cm), or in a square central area (120 cm x 120 cm), or in the 30-cm edge strip (see Figure 2B). To assess time stability, in Figure 3C speed scores were computed using data from 10-minute blocks within the same session. In Figure 2D, speed scores were computed using data within 10-minute blocks when the animal was located in a specific arena subregion.

Speed-binned autocorrelogram

To compute the speed-binned autocorrelograms shown in Figure 4A, we linearly interpolated animal speed to match the LFP sampling rate (1,250 Hz) and counted neuronal spikes at the same resolution. The interpolated speed time series was binned into overlapping bins (bin width = 5 cm/s, bin step = 2 cm/s). For each speed bin, we only considered periods of at least 625-ms in which the animal's speed did not outmatch the corresponding speed range for more than 125 ms. Next, for each selected period we computed the LFP and spike count autocorrelograms. Finally, the speed-binned autocorrelograms were obtained by plotting the mean autocorrelograms for each speed bin, normalized by its integral.

Spike count per theta cycle

To compute the number of spikes per theta cycle, we bandpass filtered the LFP between 4 and 12 Hz. For each session, we selected the electrode with the highest theta power. The instantaneous theta phase was obtained from the analytical representation of the signal based on the Hilbert transform. Downward crossings defined boundaries between theta cycles. For each theta cycle, we computed the mean animal speed and the number of spike counts per neuron.

Neuron type classification

We inherited the neuronal type classification as provided along with the hc-3 dataset, which was performed as described in Mizuseki et al. (2009). In brief, hippocampal neurons were classified as either pyramidal neurons or interneurons based on waveform width,

mean firing rates (Csicsvari et al., 1999) and auto-correlograms (Sirota et al., 2008). Moreover, monosynaptic interactions between pairs of neurons were inferred by the analysis of cross-correlograms as described in detail in Fujisawa et al. (2008). In Figures 5, 6, 7, S1, and S7, we only considered neurons that were confirmed to be excitatory or inhibitory by the latter cross-correlogram analysis.

Linear decoders

In Figures 6 and S2, we built linear models using animal speed and firing rates as response and predictor variables (Kropff et al., 2015). For these analyses, animal speed and firing rates were averaged over 1 s non-overlapping bins. For each session, the first 350 samples were used for training the model and the following 150 samples for testing. In Figure 6D, the number of neurons employed varied from one to four in a given session. The number of models for each session was determined by all possible combinations of cells. For each model, the "decoding accuracy" was defined as the Person's r squared (r^2) computed between observed and predicted speeds. In Figure S2, training and testing samples were derived from either the same or different sessions, as labeled; the mean decoding error was defined as the average difference between predicted and observed speeds. In Figure 6E, before computing single cell decoding accuracy and speed scores as above, we randomly down-sampled spikes in order to make the two cell types have the same average firing rate, as indicated in the x axis. This procedure was performed 100 times for each cell and fixed firing rate value. For the statistical analysis (mean, SEM and t test), we used the average value of a cell as a sample.

Computational models of place and speed cells

We used original behavioral data (position and speed) to simulate the instantaneous firing rate of model place and speed cells, derived from a Poisson process of mean λ. For each recorded session, the animal position was binned into 10-cm wide bins and the instantaneous speed into 8 quantiles. For model place cells, the mean firing rate (λ_{place}) was solely a function of space, determined by a "spatial tuning curve." For model speed cells, the mean firing rate (λ_{speed}) was a function of speed, determined by a "speed tuning curve." Different model cells were simulated using different tuning parameters. In the square arena, the spatial tunings were 2D-Gaussians with center coordinates (x,y) $\in$ {(90,90),(126,54),(18,90),(18,18)} (cm,cm) and standard deviation (σ_x,σ_y) $\in$ {(45,45),(27,27),(9,9)} (cm,cm); in the linear arena, we used 1D-Gaussians with x $\in$ {70,125,236} cm and $\sigma_x \in$ {45,27,9} cm. The speed tuning curves were sigmoid functions with rising constant of 20 cm/s and half constant $\in$ {20,35,50} cm/s in the square arena and $\in$ {20, 45, 70} cm/s in the linear arena. Finally, for both λ_{place} and λ_{speed}, the tuning curves were normalized such that the maximal and minimal values (λ_{min},λ_{max}) $\in$ {(0,1),(0,10),(0,40),(40,80)} (Hz,Hz). In Figures S4 to S6, we also investigated mixed neuron types, in which the mean firing rate was first set to $\lambda_{s:p} = s\lambda_{speed} + p\lambda_{place}$, with (s,p) $\in$ {(4,0),(3,1),(2,2),(1,3),(0,4)} and then normalized to achieve the desired (λ_{min},λ_{max}) values. Simulated firing rates were analyzed in the same way as the actual firing rates.

Linear-nonlinear algorithm

To control for the ethological interdependence of spatial position and speed (e.g., speed is lowest on the edges of the linear arena), in Figures S6 and S7 we used the linear-nonlinear (LN) statistical model described in Hardcastle et al. (2017). LN models can be used to quantify the dependence of the firing rate on position and speed isolatedly or in combination (Hardcastle et al., 2017). Briefly, LN models estimate the mean firing rate of a neuron as the exponential of the weighted sum of the analyzed variables. For models that take into account both position and speed, mean neuronal activity is estimated as:

$$\mathbf{R} = \exp(\mathbf{P} * \mathbf{w_p} + \mathbf{S} * \mathbf{w_s}),$$

while $\mathbf{R} = \exp(\mathbf{P} * \mathbf{w_p})$ or $\mathbf{R} = \exp(\mathbf{S} * \mathbf{w_s})$ for single variable models. $\mathbf{R}$ is a T x 1 vector of mean firing rate values, T the number of 25.6-ms time bins, $\mathbf{P}$ and $\mathbf{S}$ are T x n_p and T x n_s matrices, where n_p is the number of position bins (n_p = 36 and 50 for the square and linear arenas, respectively) and n_s the number of speed bins (we used 7 evenly distributed speed bins). Each column (a time bin) of $\mathbf{P}$ or $\mathbf{S}$ has one entry equal to 1 at the bin corresponding to the animal position or speed and 0 otherwise; $\mathbf{w_p}$ and $\mathbf{w_s}$ are weight column vectors with n_p and n_s rows. These weights are learned through an optimization algorithm that maximizes the Poisson log-likelihood (Hardcastle et al., 2017). Predicted firing rate time series are generated through Poisson processes with mean rate parameter at each time bin determined by $\mathbf{R}$. Model performance is characterized by the log-likelihood increase (LLHi) of the data under the model in relation to a Poisson model of fixed firing rate, and by the accuracy (r^2) of the model in predicting the real spiking activity of the neuron. To compute the latter, the spike counts generated by the model were smoothed as the actual data. Implementation was done by adapting codes available at https://github.com/GiocomoLab/ln-model-of-mec-neurons/ (last commit on 29 October 2017).

QUANTIFICATION AND STATISTICAL ANALYSIS

Speed scores were defined as the Pearson product-moment correlation coefficient between the time series of locomotion speed and firing rate. The surrogate distributions of speed scores shown in Figure 3 were obtained by computing the Pearson correlation coefficient between animal speed and the firing rate time series randomly circularly shifted between $\pm$ 90 s. Speed cells were operationally defined as neurons whose absolute speed score was higher than 0.3. The p values associated with the Pearson's correlation coefficients shown in Figures 1D, 2C, 2D, and 4C were obtained using Student's t distributions (function corr.m in MATLAB).

The cross-correlation lags in Figure S1 were compared against zero using one-sample t tests. Mean decoding accuracy obtained for pyramidal cells and interneurons (Figures 6D and 6E) was compared with two-sample t tests. In Figure 7C, the speed scores for the preferred and non-preferred directions were compared with paired t tests; the proportion of bidirectional speed cells among interneurons and pyramidal cells were compared using a chi-square test. In all statistical analyses, $p < 0.05$ was considered to be statistically significant. Unless noted otherwise, data from individual neurons were considered as samples.

DATA AND SOFTWARE AVAILABILITY

The HC3 dataset has been deposited in the CRCNS (http://crcns.org/data-sets/hc/hc-3).

Cell Reports, Volume *25*

Supplemental Information

Characterizing Speed Cells in the Rat Hippocampus

Zé Henrique T.D. Góis and Adriano B.L. Tort

Supplementary Figures

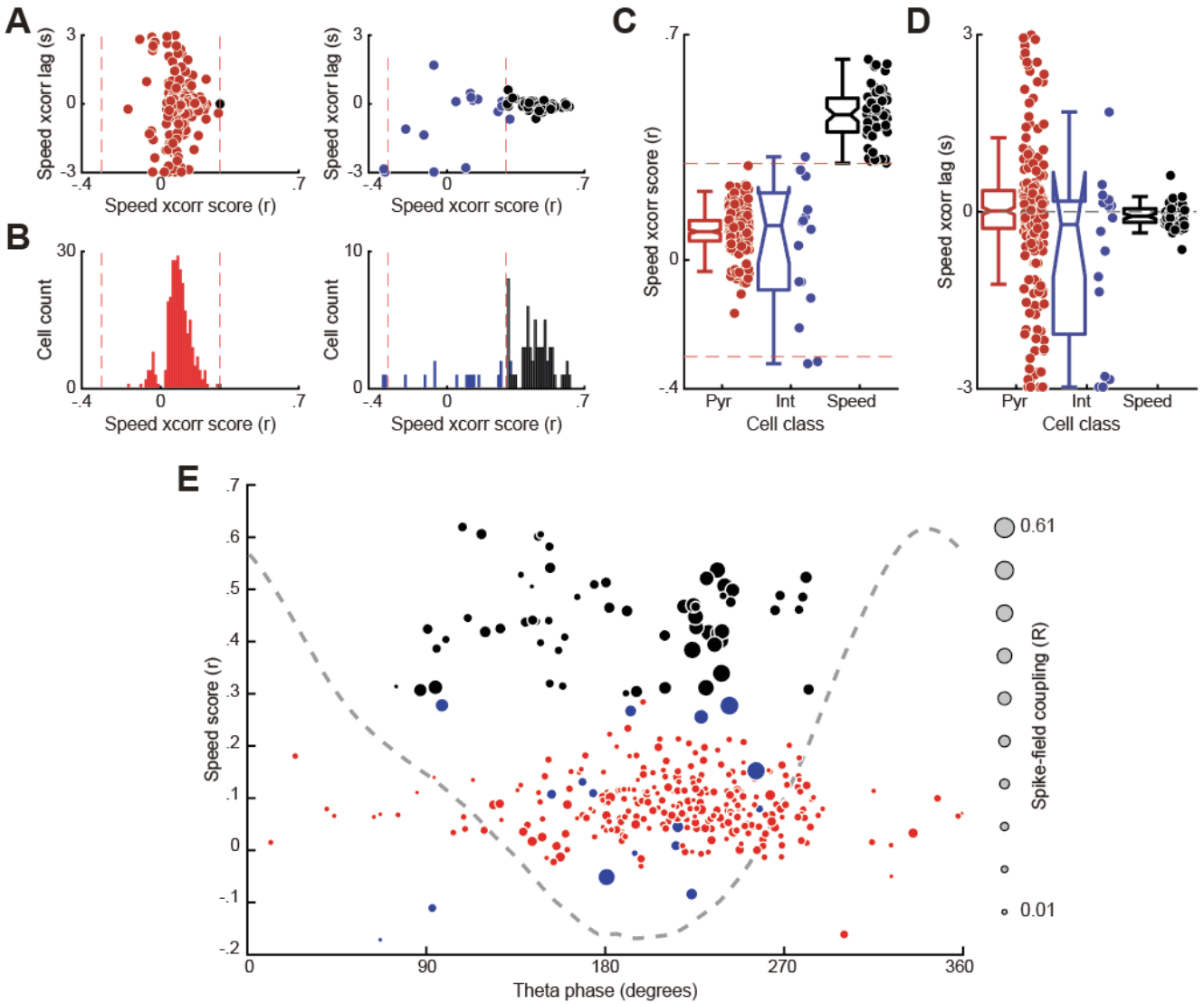

Figure S1 (Related to Figure 5). CA1 speed cells are interneurons.

(A) Scatter plots of the time lag ("speed xcorr lag") vs. the peak ("speed xcorr score") of the cross-correlation between firing rate and locomotion speed, shown separately for physiologically identified pyramidal cells (left) and interneurons (right). Units classified as speed cells in the square open-field arena by the standard speed score (xcorr at 0 lag) are shown in black, whereas other interneurons and pyramidal cells (i.e., non-speed cells) are shown in red and blue, respectively.

(B) Histogram counts of speed xcorr scores.

(C and **D)** Boxplot distributions of speed xcorr score (C) and speed xcorr lag (D) for speed cells ("Speed") as well as for other interneurons ("Int") and pyramidal cells ("Pyr") that are not speed cells.

(E) The scatter plot shows the preferred spiking phase vs the standard speed score for each cell. Circle size indicates the strength of spike-phase coupling (R: mean vector length).

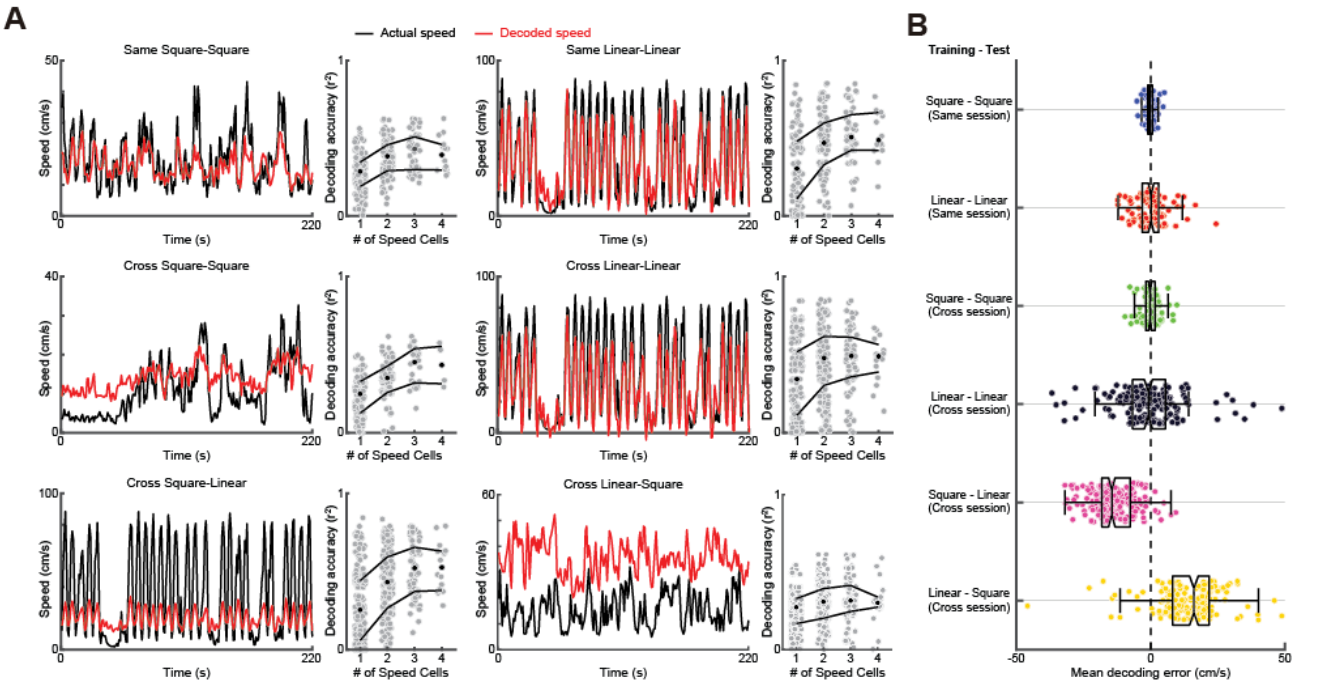

Figure S2 (Related to Figure 6). Speed decoding from the firing rate of CA1 speed cells.

(A) On each column, the left panels show the time series of observed (gray) and decoded (red) speed from the firing rate of an individual CA1 speed cell. Linear decoders were trained using 350 seconds of data distinct from the 150-second testing period. Decoders were trained in one session and tested using either the same session ("Same") or another session ("Cross") recorded in the same day; the training and testing session arenas are stated in the title. The right panels show mean decoding accuracy for all possible models with the same fixed number of neurons within a session. Decoders were trained with 1 to 4 CA1 speed cells. Gray circles show individual sessions; black circles and lines show the median and 25-75% quartiles.

(B) Boxplot of the mean difference between decoded and observed speeds for decoders trained with only one CA1 speed cell. Decoding error centered near zero when using training and test data from the same arena, and it was negative when the decoder was trained with data from the square arena and tested with linear track data; the opposite happened when using training and test data from the linear and square arenas, respectively, in which case the mean decoding error was positive. These results relate to the fact that animals achieved higher locomotion speeds in the linear track than in the square arena.

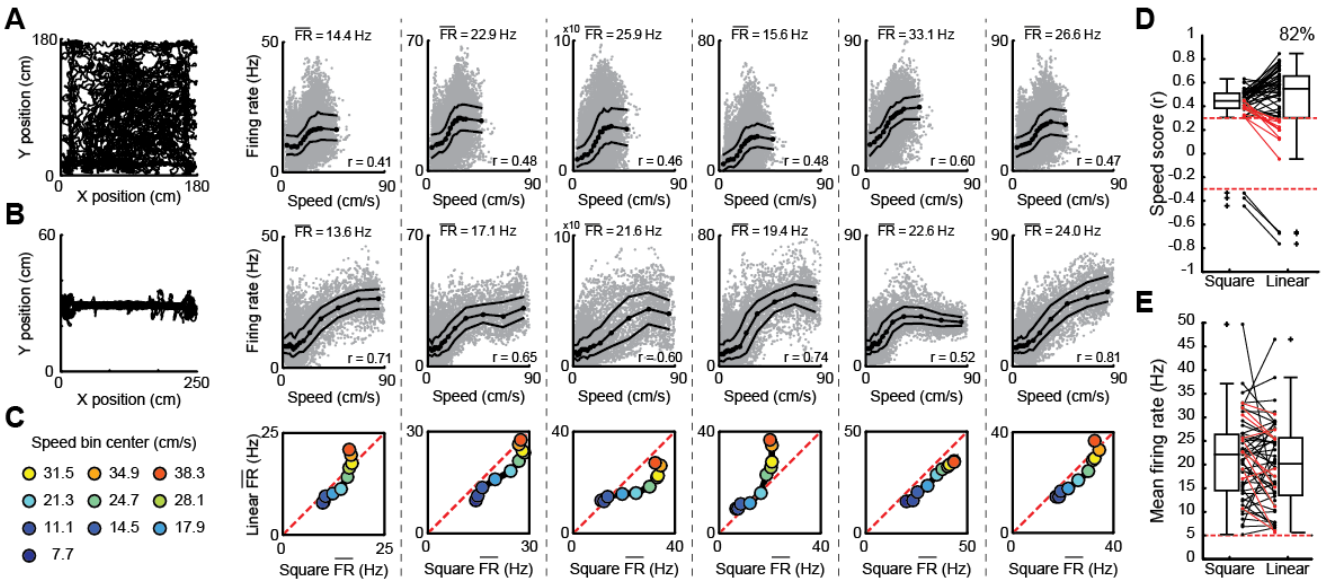

Figure S3 (Related to Figure 7). CA1 speed cells defined in the square arena are also speed cells in the linear track.

(A, B) Animal tracking and scatter plots of speed vs. firing rate of six CA1 speed cells recorded in the same day in the square (ec013.858) and linear (ec013.859) arenas. Black circles and lines show the median and 25-75% quartiles for each speed bin. Inset texts indicate speed scores (all p's<10^{-20}); the titles state the mean firing rate ($\overline{FR}$).

(C) Scatter plots of speed binned $\overline{FR}$ in the square vs. linear arenas (same cells as in A and B). Colors indicate speed bin centers (bin width = 3.4 cm/s).

(D) Boxplot of speed scores in the square and linear arenas for CA1 speed cells defined in the square arena; 82% of the cells were also considered speed cells in the linear track (red lines mark unstable cells). Only cells with firing rate > 5 Hz in both arenas were taken into account.

(E) Boxplot of $\overline{FR}$ for the same cells as in D.

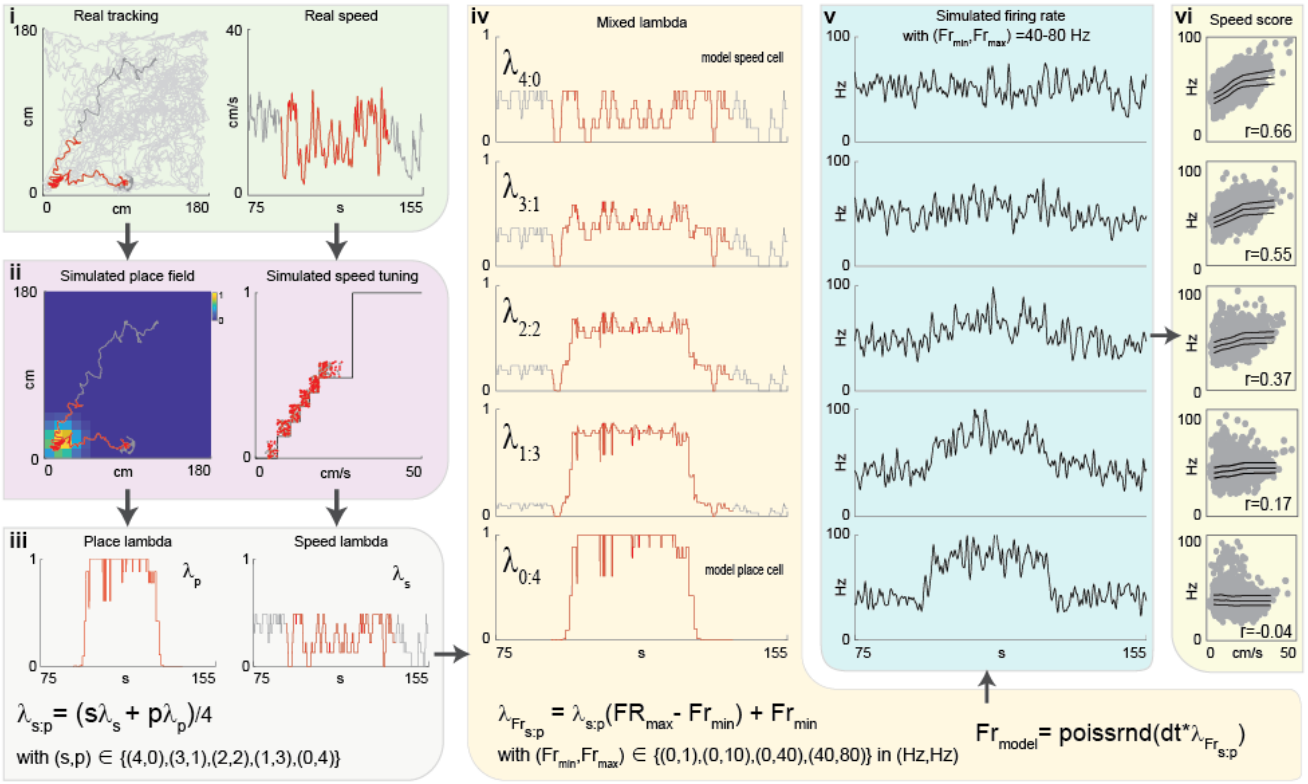

Figure S4 (Related to Figure 7). Computational models of speed and place cells.

(i-vi) Computational models were implemented using the actual animal position and speed (i), which, based on simulated spatial and speed tuning curves (ii), determined the instantaneous values of the place (λ_p) and speed (λ_s) rate parameters (iii). We simulated five types of neuronal activity: model place or speed cells, which had firing rate solely determined by λ_p or λ_s, respectively, as well as three mixed neuron types which had firing rate determined by a weighted sum of λ_p and λ_s (iv). The weighted rate parameters were normalized to be bounded between minimal and maximal values of choice. Finally, the instantaneous firing rate of the model cells was simulated as the outcome of a Poisson process (v) and used to compute the speed score (vi).

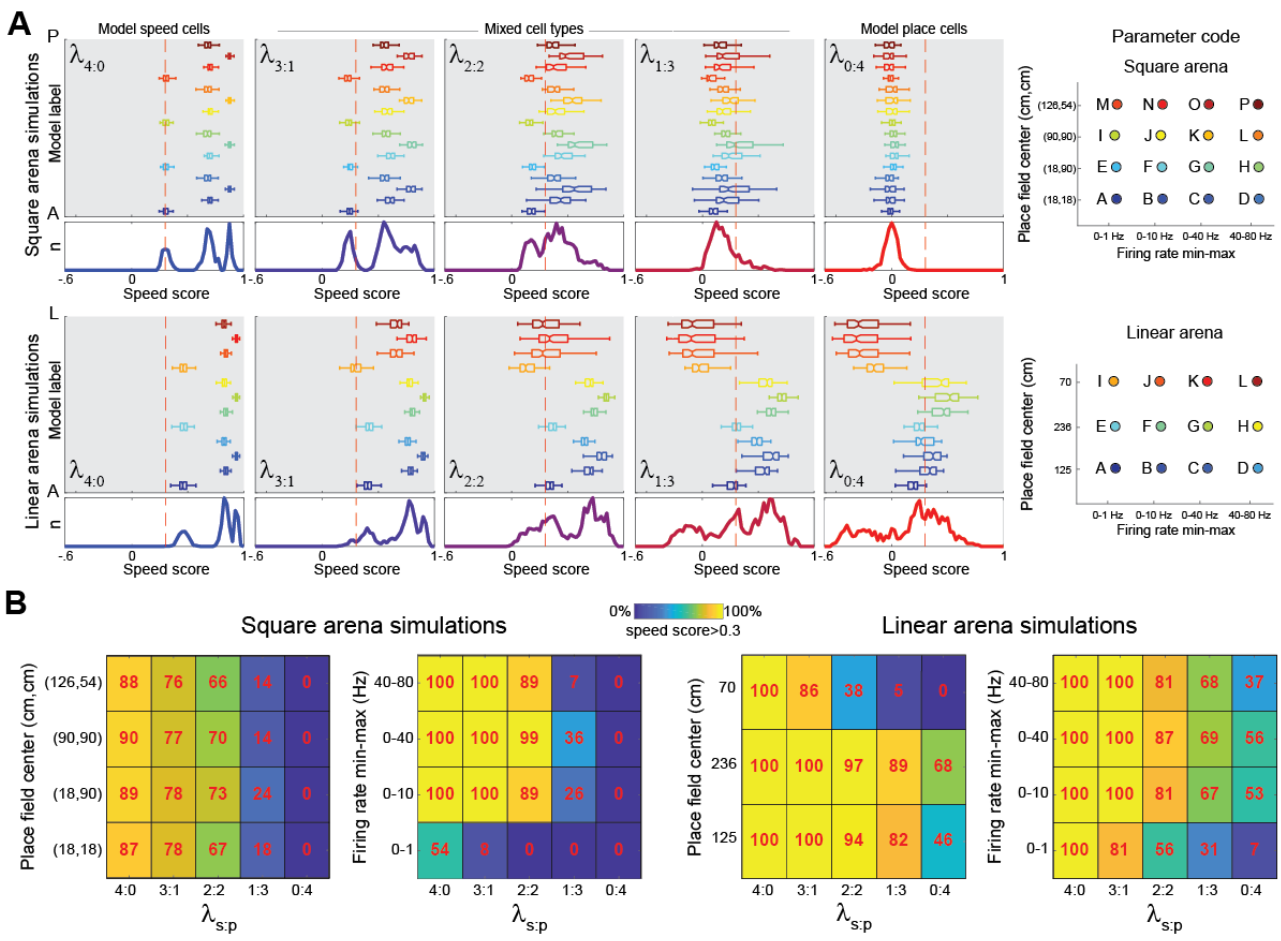

Figure S5 (Related to Figure 7). Computational models of place cells spuriously correlate with speed in the linear track.

(A) Distribution of speed scores for model neurons simulated with different parameters (color/letter code on the right). Simulations were implemented using actual behavioral data (position and speed) from square open-field arena (top) or linear track (bottom) sessions. The different columns show results for model neurons with different levels of speed and place coding, from pure speed cells ($\lambda_{4:0}$) to pure place cells ($\lambda_{0:4}$) (see Figure S4).

(B) Percentage of model neurons considered speed cells by the operational definition (speed score>0.3). In each panel, the leftmost and rightmost columns show results for pure speed and place cells, respectively. Notice in the linear track that a high percentage of pure place cells ($\lambda_{0:4}$) are deemed speed cells even though no speed coding was simulated for these cells.

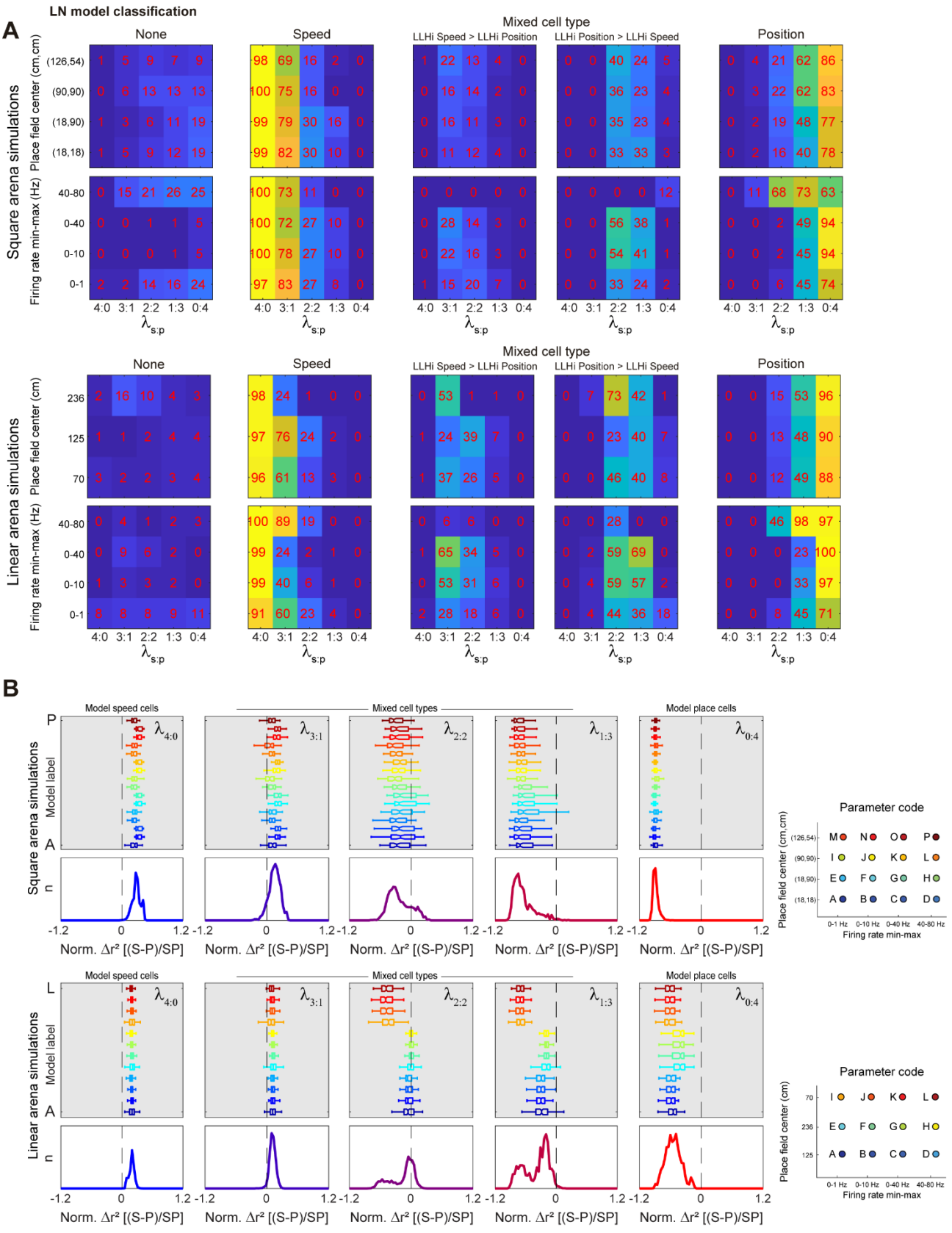

Figure S6 (Related to Figure 7). Statistical LN models correctly classify simulations of place and speed cell models.

(A) Simulations of place and speed cells were performed as in Figures S4 and S5. Linear-nonlinear-Poisson (LN) models were used to classify coding properties of the simulated neurons (see Method Details and Hardcastle et al., 2017). Cells were classified as having no coding preference ("None") when the log-likelihood increase (LLHi) for LN speed models and LN position models in relation to a Poisson model of fixed firing rate was not significantly higher than 0. Otherwise, cells were classified as "Speed" or "Position" depending on the significance of the corresponding LLHi. The "Mixed cell type" classification denotes cells whose LLHi of LN speed & position models was statistically significantly higher than the LLHi of isolated LN position or LN speed models. Notice that most of pure speed cells ($\lambda_{4:0}$) and pure place cells ($\lambda_{0:4}$) were correctly classified as such in either arena.

(B) Normalized difference in firing rate prediction accuracy (Δr^2) between speed and position LN models (as in Figure S7E) for simulations in the square and linear arenas (as in Figure S5). Positive values denote better prediction by speed, and negative values, by position.

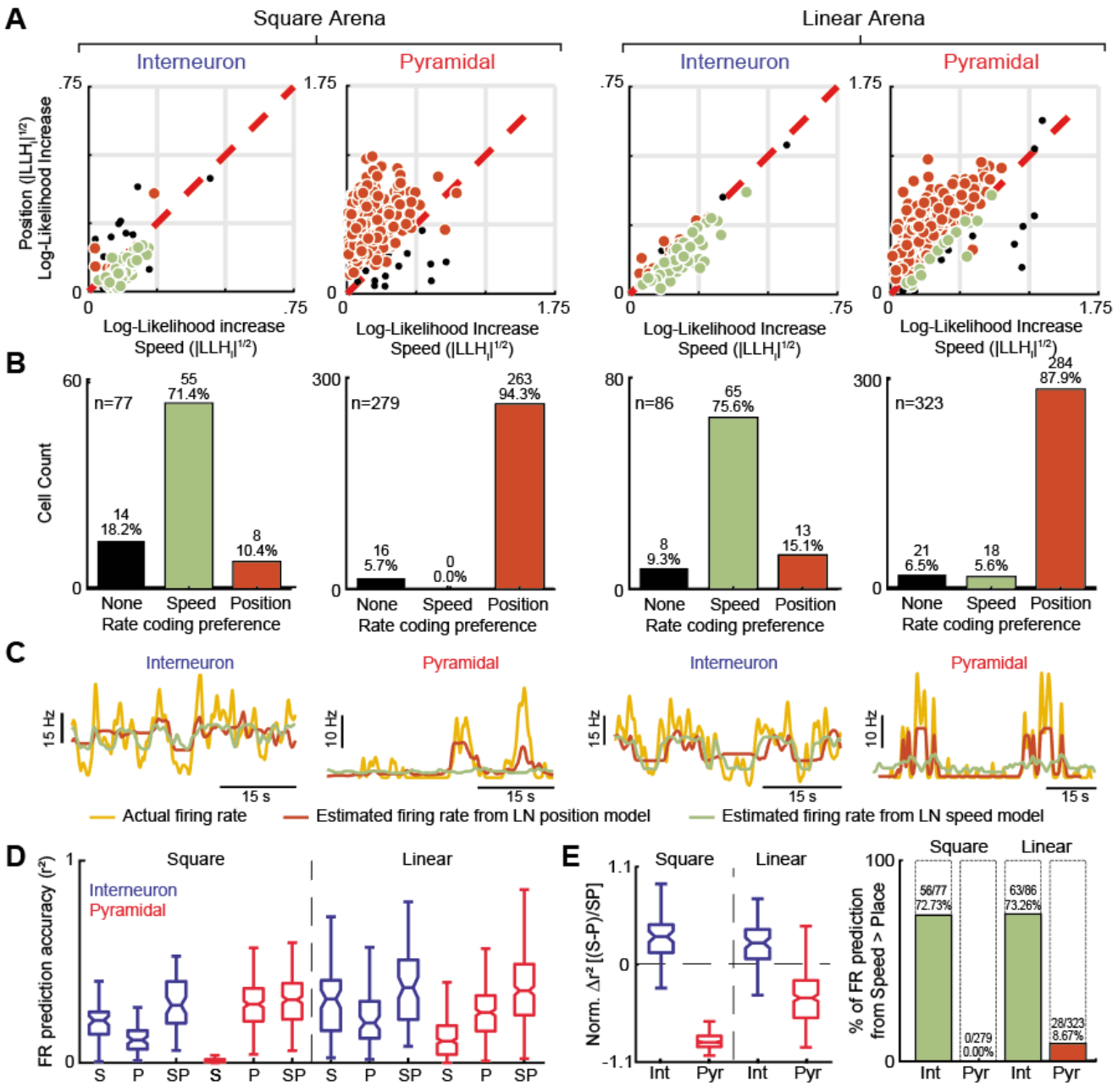

Figure S7 (Related to Figure 7). Statistical LN models reveal preferential encoding of speed by interneurons and of space by pyramidal cells.

(A) Scatter plots of the log-likelihood increase (LLH_i) for LN firing rate models considering position (y-axis) or speed (x-axis) in comparison to a fixed mean firing rate model. Results plotted separately for each arena and cell type, as labeled. Green and orange circles denote cells whose firing rate was better explained by speed or position, respectively; black circles show cells without statistically significant influence of either variable.

(B) Percentage of cells preferentially modulated by speed (green) or position (orange), as defined by the highest significant LLH_i. The percentage of non-modulated cells (non-significant LLH_i) is also shown (black).

(C) Examples of firing rate time series plotted along with the predicted firing rate time series from LN models based on the instantaneous position or speed. Notice that the pyramidal cell firing rate is not well fitted by the LN speed model in either arena.

(D) Prediction accuracy for LN models based on speed (S), position (P) or both variables (SP), defined as the coefficient of determination (r^2) between the predicted and the actual firing rate (FR) time series.

(E) (Left) Normalized difference in FR prediction accuracy (Δr^2) between speed and position LN models. Positive values denote better prediction by speed, and negative values, by position. (Right) Percentage of cells whose FR was better predicted by speed than position.